

# Global Navigation Using Predictable and Slow Feature Analysis in Multiroom Environments, Path Planning and Other Control Tasks

Stefan Richthofer\*, Laurenz Wiskott†

*Institut für Neuroinformatik,  
Ruhr-Universität Bochum, Germany*

May 23, 2018

## Abstract

Extended Predictable Feature Analysis (PFax) [Richthofer and Wiskott, 2017] is an extension of PFA [Richthofer and Wiskott, 2015] that allows generating a goal-directed control signal of an agent whose dynamics has previously been learned during a training phase in an unsupervised manner. PFax hardly requires assumptions or prior knowledge of the agent’s sensor or control mechanics, or of the environment. It selects features from a high-dimensional input by intrinsic predictability and organizes them into a reasonably low-dimensional model.

While PFA obtains a well predictable model, PFax yields a model ideally suited for manipulations with predictable outcome. This allows for goal-directed manipulation of an agent and thus for local navigation, i.e. for reaching states where intermediate actions can be chosen by a permanent descent of distance to the goal. The approach is limited when it comes to global navigation, e.g. involving obstacles or multiple rooms.

In this article, we extend theoretical results from [Sprekeler and Wiskott, 2008], enabling PFax to perform stable global navigation. So far, the most widely exploited characteristic of Slow Feature Analysis (SFA) was that slowness yields invariances. We focus on another fundamental characteristics of slow signals: They tend to yield monotonicity and one significant property of monotonicity is that local optimization is sufficient to find a global optimum.

We present an SFA-based algorithm that structures an environment such that navigation tasks hierarchically decompose into subgoals. Each of these can be efficiently achieved by PFax, yielding an overall global solution of the task. The algorithm needs to explore and process an environment only once and can then perform all sorts of navigation tasks efficiently. We support this algorithm by mathematical theory and apply it to different problems.

---

\*Electronic address: [stefan.richthofer@ini.rub.de](mailto:stefan.richthofer@ini.rub.de); Corresponding author

†Electronic address: [laurenz.wiskott@ini.rub.de](mailto:laurenz.wiskott@ini.rub.de)

# 1 Introduction

The original motivation of this work is based on the idea to apply the unsupervised learning algorithm Slow Feature Analysis (SFA) [Wiskott and Sejnowski, 2002] to interactive scenarios. The motivation for this idea is based on the experience that SFA was successfully used in various (passive) analysis tasks that closely relate to such scenarios, e.g. learning place cells [Franzius et al., 2007, Schönfeld and Wiskott, 2015], identifying objects invariant under spacial transformations [Franzius et al., 2008, Berkes and Wiskott, 2002, Franzius et al., 2011], blind source separation [Sprekeler et al., 2014], visual tasks like face recognition and age estimation [Escalante-B. and Wiskott, 2013]. In previous work, we recognized predictability as a crucial feature for tackling interactive scenarios, as these require estimation of consequences of possible actions. This led to the invention of Predictable Feature Analysis (PFA) [Richthofer and Wiskott, 2015, Richthofer and Wiskott, 2017], an algorithm strongly inspired by SFA – while SFA selects features by slowness, PFA selects them by predictability. Before we get into more detail of these algorithms, we briefly collect possible application fields.

Path planning of mobile robots is an application area that closely fits our implicit prototype assumptions. We imagine a robot in an environment that perceives sensory input of some kind and emits an action signal that controls its motors (c.f. Figure 1). A naturally arising task is to control the robot such that it reaches a desired state in the environment.

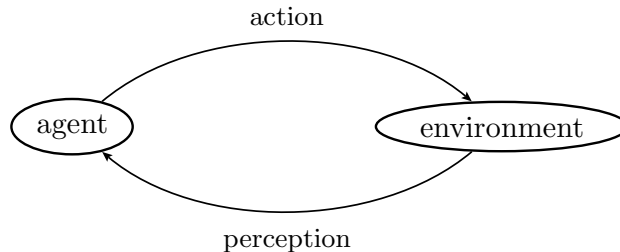


Figure 1: Perception/action cycle

SFA has been frequently applied to model a rather similar scenario concerning a rat instead of a robot. Of course, it was not attempted to control the rat, but to obtain biologically plausible phenomena like place cells. A more general interactive problem setting is reinforcement learning (RL), where also an agent is acting in an environment, aiming for a maximal accumulated reward over time. In this fashion, that setting extends our notion of a sensor signal and a control signal by a reward signal. Also control theory of dynamical systems, involving tasks like pendulum swing up, pole and cart balancing, fits into the notion of an action/perception loop illustrated in figure 1. The phase space of the system can be seen as environment in this case. A rich repertoire of work exists that links these fields in various ways. Traditionally, RL algorithms are applied to path planning, or dynamical systems. We list a selection of such articles throughout this section.

As a unifying notion of the named areas' essentials we stick to the idea of controlling an agent in an environment, aiming for a specific goal state. Environment, agent and control are represented as abstract, continuous sensor and control signals. Based on this, we perceive the navigation into a goal state as an optimization problem. This matches the setting we tackled with PFAx in [Richthofer and Wiskott, 2017] and we continue with a comprehension of that approach.

## 1.1 Predictable Feature Analysis (Extended)

Predictable Feature Analysis (PFA) [Richthofer and Wiskott, 2015] is an unsupervised learning algorithm that was developed to efficiently turn high-dimensional input data into a low-dimensional model consisting of well predictable features.

In [Richthofer and Wiskott, 2017] we have shown that by using an extension to PFA – namely PFAX – it is possible to learn well controllable features that are sufficient to solve local navigation tasks. By taking supplementary information into account for prediction, PFAX can find features that are ideally predictable based on themselves and under the assumption that a supplementary signal can be used as a helper for prediction. Such a supplementary signal does – however – not participate in feature extraction. Providing the control signal from the RL setting (specific action chosen at each time-step) as supplementary information, we can obtain features that strongly depend on the supplementary information in terms of predictability. By inverting that relation we can compute the control signal that would most likely yield a specific desired outcome, given the agent’s current state. In this sense the obtained features are well controllable.

Solving a complex navigation task usually cannot be achieved within a single time step, so we transformed the agent’s state as far as possible towards the goal state in each time step (greedy optimization), using least squares distance in feature space as a cost function. The resulting approximate gradient descent easily gets stuck in a local optimum, thus PFAX is only suitable to perform local navigation.

## 1.2 Approach in this work

A key observation is that Slow Feature Analysis (SFA) [Wiskott and Sejnowski, 2002] can be used to decompose a given environment into features that are represented as monotonic signals across the environment (see [Sprekeler and Wiskott, 2008]). We refer to these monotonic features as *sources*. Computing them from the usual slow features found by SFA requires additional processing. This is provided by the xSFA algorithm [Sprekeler et al., 2014]. The theoretical analysis of xSFA only scopes the case that statistically independent sources exist. We extend this analysis in section 3.2 and establish a geometrical characterization of the solutions in terms of potential, monotonicity, geodesics and representation of the data manifold. A major contribution of this work is to clarify what (x)SFA-induced monotonicity means in higher dimensions. These results motivate the navigation algorithm proposed in section 3.3.

Obtaining the sources involves an extensive unsupervised exploration phase in which PFAX can learn the effects of the control signal and (x)SFA can learn a model of the environment. Based on the learned representation, any navigation problem can be solved by local descent on the monotonic feature representation, using the learned effects of the control signal. In figure 2 we illustrate this with the interval  $[0, 100]$  serving as a 1D environment. As a sensor representation we model five differently parametrized grid cells using overlapping Gaussians. The component (*sfl*) obtained by xSFA yields a monotonic representation of the environment. Concerning the goal distance measures on the right, imagine we wanted to move an agent from e.g. position 80 to the goal at 40. Based on local techniques (imagine a limited perception range, e.g. one or two units) it is impossible to efficiently find the goal regarding sensor space. Measuring distance by *sfl*, the same task – actually any navigation task – is well feasible.

A special case of the approach in this work was studied in [Metka et al., 2017]. Leveraging the monotonicity of the slowest SFA components, a robot is navigated in an approximately open

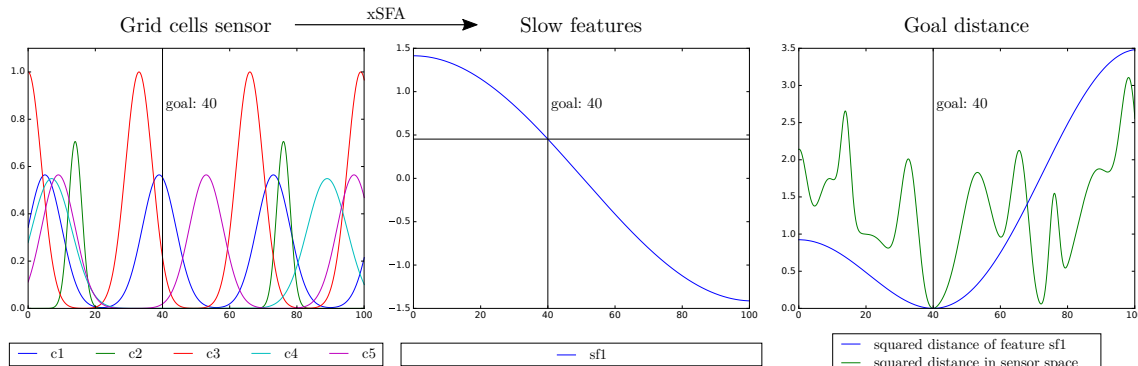


Figure 2: Illustration of how xSFA obtains a cost function suitable for efficient global optimization on  $[0, 100]$ . *Left*: Overlapping Gaussians are used to model grid cells as non-monotonic representation. *Center*: Results of xSFA applied to the representation on the left. The extracted component (*blue*) yields a monotonic representation of the environment. *Right*: Comparison of goal distance functions. Squared goal distance in sensor space (*green*) *cannot* be optimized globally by local methods. Squared goal distance in feature space (*blue*) *can* be optimized globally by local methods.

environment around an obstacle. This asserts the feasibility of the method in principle. A major difference to the approach presented here is that the control of the robot is not learned, but assumed to be known. Also the estimation of the gradient is done in a different manner. The navigation is based on a fixed selection of SFA components, which limits it to environments yielding spatial dimensions of roughly the same size, e.g. with quadratic or circular boundary. In that sense, our paper presents a generalization of that approach, vastly relaxing the geometrical requirements on the environment. However, we still require some non-geometric limitations on the environment:

- The environment is fully observable, i.e. each position in the environment yields a unique representation in sensor space
- The environment is stationary, i.e. constant over time, contains no blinking lights, no flickering colors or moving objects

The named limitations are not inherent and in section 5.2 we suggest extensions of the algorithm to overcome each of them. They are just simplifying assumptions to focus on the core method in this work.

### 1.3 Connection to optimization

Using a distance measure (e.g. least squares distance in sensor or feature space) of the agent's current state to a goal state as a cost function, a navigation task can be seen as an optimization problem. Complex tasks usually cannot be achieved within a single time step. This can be resolved in several ways, e.g.:

- An optimization problem could be defined on the space of possible paths rather than on a space of possible actions.

- Greedy optimization can be used, i.e. transforming the agent’s state as far as possible towards the goal state in each time step (c.f. gradient descent).
- Optimization can scope on finding a good policy.

Finding a policy is the typical approach in RL, which is discussed in the next section. Greedy optimization easily gets stuck in a local optimum and finding the globally optimal path in an arbitrary environment is a general black-box global optimization problem. Without further assumptions on the environment, such a problem would in general not be convex, quadratic or anything significantly useful. Historically, a wide range of techniques has been developed to deal with such black-box problems, e.g. evolutionary algorithms, swarm algorithms, convex relaxations, cutting plane methods, branch and bound methods, stochastic methods and many more. These techniques have in common that they are magnitudes slower than methods for efficiently optimizable problem domains like convex, quadratic or linear problems. Apart from that, they usually cannot guarantee convergence or actual optimality of the obtained result.

The method in this work can be seen as a reverse approach applicable to our specific setting. Instead of attempting to solve the resulting difficult optimization problem, we create the optimization problem such that it is efficiently solvable. Given that we already use a model to represent the agent’s state, we have a certain degree of freedom in forming this model. The presented method can intentionally form the model such that all possible goal states in the environment are efficiently achievable from any initial state.

In this context, we exploit SFA-induced monotonicity as a link between local and global optimization: Exactly on monotonic functions, the distance measure to a goal value has only a single optimum. Thus, exactly on these functions, local techniques like PFAx are sufficient for global optimization of goal-distance. However, for multidimensional environments there does not exist a single strictly monotonic component that can cover all possible goal states. Instead we will find a hierarchical decomposition into components to cover the whole environment, defining a precise sequence of efficiently and globally solvable optimization tasks to reach any desired goal state that exists in the environment, provided that it has been sufficiently explored.

## 1.4 Connection to Reinforcement Learning

Navigating an agent in an environment has significant links to RL. However, RL usually considers an arbitrary reward signal, typically in discrete state and action spaces, while approaches for continuous RL exist. Navigation tasks and path planning can be encoded in the RL setting by measuring the distance of the agent’s current state from the goal state by a certain metric (e.g. euclidean distance in sensor or feature space). Using an inversion of this measure (e.g.  $\frac{1}{x}$  or  $\max -x$ ) as reward function would yield maximum reward at the goal. The main formal difference to the optimization view is that the objective function, i.e. the accumulated future reward, in RL terms the *value function* is unknown and is usually learned in popular methods such as Q-Learning. Apart from that, having a reward function that is non-zero across wider ranges of the environment is untypical for RL. Usually reward is only given right at the goal and the value function is learned across multiple sessions.

In terms of RL, the approach in this work would mean that during an initial exploration phase, reward would be completely ignored and instead the topology of the environment and the dynamics of the agent would be exhaustively learned. Based on this, any reward signal that measures distance to some goal position can be maximized efficiently. Goal and start position can be arbitrary and

any number of such tasks with varying start and goal can be performed efficiently based on a single initial exploration. This is possible, because the model is aligned to the environment and not the specific reward function. Thus, our approach is especially valuable if the goal is not known during exploration and if many tasks with different goals need to be performed in the same environment. Note that in terms of RL, our approach does not account for the exploration-vs-exploitation issue. It rather performs exhaustive exploitation after exhaustive exploration.

Proto value functions (PVFs) [Mahadevan and Maggioni, 2007] are an RL concept that shares some characteristics with the presented approach. They are frequently used to discover bottleneck states and options in RL settings. SFA has been used earlier to approximate PVFs, e.g. in [Luciw and Schmidhuber, 2012, Böhmer et al., 2013]. The extracted slow features can then be used as basis functions for linear models that solve the RL problem, such as LSTD [Lagoudakis et al., 2002].

Originally, the central building block of PVFs are Laplacian eigenmaps (LEMs) rather than slow features. LEMs are traditionally more affected by the curse of dimensionality in RL as the dimensionality of the graph Laplacian depends on the number of data points. [Sprekeler, 2011] provides the missing link between SFA and LEMs. Specifically, that work identifies conditions under which the problem settings of SFA and LEMs become equivalent and describes how LEMs can be approximated by slow features. The application of SFA as replacement for LEMs proposed in [Luciw and Schmidhuber, 2012, Böhmer et al., 2013] was originally enabled by the named article. For our purpose, slow features yield another crucial advantage over LEMs: SFA’s central optimization problem can be analyzed by Sturm-Liouville theory, which allows to formally prove monotonicity results for slow features [Sprekeler and Wiskott, 2008].

In this work we primarily take the optimization perspective onto the navigation setting. Our approach is rather driven by xSFA and its theoretical implications and we propose that based on results of a sufficiently converged xSFA processing, it is already feasible to fully solve our setting by local and efficient optimization techniques.

## 1.5 Connection to path planning

Path planning of mobile robots closely fits our assumed setting as it deals with finding a safe path to navigate a robot through a complex environment. Work in this area usually assumes a specific goal location. A key difference is that the robot’s dynamics are usually known and focus is fully on planning the path. Our approach on the other hand does not incorporate a safety criterion, but this could be modeled as an additional part of the sensor.

The optimization issues we stated in section 1.3 are widely recognized in this field, especially avoidance of local optima is a central concern [Warren, 1989]. We pointed out the nature of a black box optimization problem and indeed various typical black box optimization approaches have been applied to path planning: Evolutionary methods [Vadakkepat et al., 2000], neural networks [Engedy and Horvath, 2009], particle swarm optimization [Kun Su and Hu, 2015], ant colony optimization [TAN et al., 2007, Xu et al., 2017] and others [Garrido et al., 2006]. Path planning has also been frequently approached using RL [Romero-Martí et al., 2016, Zuo et al., 2014, Singh et al., 1994, Igarashi, 2002, Kollar and Roy, 2008].

## 1.6 Other related work

We give an overview of various other more or less closely related approaches. Some papers are listed because they apply a hierarchical decomposition of some sort to RL scenarios, others are listed because they deal with slowness or predictability.

[McGovern and Barto, 2001] and [Stolle and Precup, 2002] use diverse density to discover bottleneck states as useful subgoals for RL tasks. This has some parallels to the algorithm in this paper in the sense that bottlenecks occur as special states. In A.2 we explicitly study the behavior of SFA around a bottleneck and suggest in a side note how slow features can be used as a bottleneck detector.

[Stachenfeld et al., 2014] suggests how a hierarchical decomposition of a problem space can be achieved using the successor representation and its eigenvalue decomposition. That work draws a number of links to studies of animal behavior, observations in the hippocampus and to cognitive maps. It contains many interesting notes regarding biological plausibility of decomposition approaches.

[Botvinick et al., 2009] addresses the scaling problem/curse of dimensionality in RL. They develop a hierarchical notion of RL (HRL) in a model-free actor-critic approach. The work features an extensive discussion of implications for neuroscience and psychology.

[Böhmer et al., 2015] gives an overview of methods for autonomous RL directly based on sensor-observations. The mainly discussed algorithms are deep auto encoders and SFA. They mention slow distractors (e.g. the position of a slowly moving sun in an outdoor scenario) as a typical issue of SFA. This supports our idea of a combination of SFA with predictability in form of PFAX, which should be able to discard slow distractors. However, PFAX can be affected by predictable distractors, but these can be identified by the coefficients of the matrix incorporating the control signal. Finally they explicitly point out the idea of combining notions of slowness with predictability, referencing the following work:

[Jonschkowski and Brock, 2013] combines notions of slowness and predictability to learn state representations for RL using a neural network. To combine these notions they propose a hybrid cost function consisting of arbitrarily weighted terms for slowness, predictability and non-constantness.

There are a number of approaches related to SFA, PFA or PFAX we discussed in a little more detail in [Richthofer and Wiskott, 2017]: Contingent Feature Analysis (CFA) [Sprague, 2014], Forecastable Component Analysis (ForeCA) [Goerg, 2013], Graph-based Predictable Feature Analysis (GPFA) [Weghenkel et al., 2017], Predictive Projections [Sprague, 2009], Neighborhood Components Analysis (NCA) [Goldberger et al., 2004], A Canonical Analysis of Multiple Time Series [Box and Tiao, 1977].

## 2 Local navigation using predictable features with supplementary information (PFAX)

We start with a comprehension of the PFAX algorithm [Richthofer and Wiskott, 2017] which extends the PFA algorithm [Richthofer and Wiskott, 2015] to incorporate supplementary information. Later we extend the method to enable global navigation. Given an  $n$ -dimensional input-signal  $\mathbf{x}(t)$ , PFA’s objective is to find  $r$  most predictable output components, referred to as “predictable features”. PFAX additionally considers a signal  $\mathbf{u}(t)$  and extracts  $r$  components from  $\mathbf{x}$  such that they are most predictable if  $\mathbf{u}$  can be used as an additional helper for the prediction.

Like SFA, PFAx performs a linear extraction, but can incorporate a non-linear expansion  $\mathbf{h}(\mathbf{x})$  as a preprocessing step. For this we usually use monomials up to a certain degree, which essentially yields a polynomial extraction overall<sup>1</sup>. Note that by the Stone-Weierstrass theorem this technique can approximate any continuous function and moreover also regulated functions (piecewise continuous). However, high degree expansion can require significant cost in terms of training data and computation. Applying PFA hierarchically like is done with SFA in [Franzius et al., 2007, Schönfeld and Wiskott, 2015] can help to keep these costs tractable.

## 2.1 Recall PFAx

In the PFAx setting, predictability is measured by **linear, auto-regressive processes** which are widely used to model time-related problems. That means, each value of an extracted signal should be as predictable as possible by a linear combination of  $p$  recent values.

This yields the problem of finding vectors  $\mathbf{a} \in \mathbb{R}^n$  and  $\mathbf{b} \in \mathbb{R}^p$  such that

$$\mathbf{a}^T \mathbf{z}(t) \stackrel{!}{\approx} b_1 \mathbf{a}^T \mathbf{z}(t-1) + \dots + b_p \mathbf{a}^T \mathbf{z}(t-p) = \mathbf{a}^T (L^1 \mathbf{z}, \dots, L^p \mathbf{z})(t) \mathbf{b} =: \mathbf{a}^T \hat{\mathbf{z}}_{\mathbf{b}}(t) \quad (1)$$

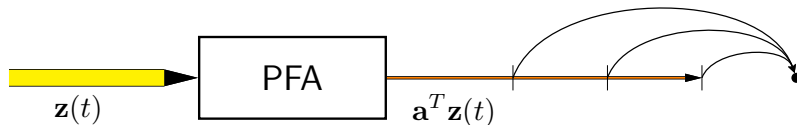


Figure 3: Illustration of PFA with extraction vector  $\mathbf{a}$ . Components are selected to be well predictable.

where  $L$  denotes the *lag operator* (also *backshift operator*), i.e.  $L^k \mathbf{z}(t) = \mathbf{z}(t-k)$ , and  $\mathbf{z}$  is the expanded representation of our input signal  $\mathbf{x}$ , sphered over a finite training phase  $\Omega_t$  with average notation  $\langle s(t) \rangle := \frac{1}{|\Omega_t|} \sum_{t \in \Omega_t} s(t)$ :

$$\tilde{\mathbf{z}}(t) := \mathbf{h}(\mathbf{x}(t)) - \langle \mathbf{h}(\mathbf{x}(t)) \rangle \quad (\text{make mean-free}) \quad (2)$$

$$\mathbf{z}(t) := \mathbf{S} \tilde{\mathbf{z}}(t) \quad \text{with} \quad \mathbf{S} := \langle \tilde{\mathbf{z}} \tilde{\mathbf{z}}^T \rangle^{-\frac{1}{2}}, \quad \mathbf{z}(t) \in \mathbb{R}^n \quad (\text{normalize covariance}) \quad (3)$$

(1) can be formulated as a least squares optimization problem over the training phase  $\Omega_t$ . We extend the problem to multiple output components  $\mathbf{a}_1^T \mathbf{z}, \dots, \mathbf{a}_r^T \mathbf{z}$  and to avoid trivial or repeated solutions we add constraints that require them to have unit variance and to be pairwise uncorrelated:

<sup>1</sup>For higher degree, Legendre or Bernstein polynomials should be favored over monomials because of better numerical stability.



For  $i \in \{1, \dots, r\}$

$$\begin{aligned}
& \underset{\mathbf{a}_i \in \mathbb{R}^n, \mathbf{b} \in \mathbb{R}^p}{\text{minimize}} && \langle \|\mathbf{a}_i^T (\mathbf{z} - \hat{\mathbf{z}}_{\mathbf{b}})\|^2 \rangle \\
& \text{subject to} && \mathbf{a}_i^T \langle \mathbf{z} \rangle = 0 \quad (\text{zero mean}) \\
& && \mathbf{a}_i^T \langle \mathbf{z} \mathbf{z}^T \rangle \mathbf{a}_i = 1 \quad (\text{unit variance}) \\
& && \mathbf{a}_i^T \langle \mathbf{z} \mathbf{z}^T \rangle \mathbf{a}_j = 0 \quad \forall j < i \quad (\text{pairwise decorrelation})
\end{aligned} \tag{4}$$

Because of the sphering  $\langle \mathbf{z} \rangle = 0$  and  $\langle \mathbf{z} \mathbf{z}^T \rangle = \mathbf{I}$ , the constraints simplify to

$$\mathbf{a}_i^T \mathbf{a}_j = \delta_{ij} \tag{5}$$

With  $\mathbf{A}_r := (\mathbf{a}_1, \dots, \mathbf{a}_r) \in \mathbb{R}^{n \times r}$ , constraint (5) is automatically fulfilled if we choose

$$\mathbf{A}_r = \mathbf{A} \mathbf{I}_r \quad \text{with} \quad \mathbf{A} \in \mathcal{O}(n) \tag{6}$$

$\mathcal{O}(n) \subset \mathbb{R}^{n \times n}$  denotes the space of orthogonal transformations, i.e.  $\mathbf{A} \mathbf{A}^T = \mathbf{I}$  and  $\mathbf{I}_r \in \mathbb{R}^{n \times r}$  denotes the reduced identity matrix consisting of the first  $r$  Euclidean unit vectors as columns.

Problem (4) is not readily solvable. As a prerequisite for a solvable relaxation we define  $\mathbf{m}(t) := \mathbf{A}_r^T \mathbf{z}(t)$  and extend the prediction model to matrix notation (7). To keep things compact we directly switch to the PFAX notion by incorporating supplementary information  $\mathbf{u}$  in (8).

$$\mathbf{m}(t) \stackrel{!}{\approx} \mathbf{B}_1 \mathbf{m}(t-1) + \dots + \mathbf{B}_p \mathbf{m}(t-p) \quad \text{with} \quad \mathbf{B}_i \in \mathbb{R}^{r \times r} \tag{7}$$

$$+ \mathbf{U}_1 \mathbf{u}(t-1) + \dots + \mathbf{U}_q \mathbf{u}(t-q) \quad \text{with} \quad \mathbf{U}_i \in \mathbb{R}^{r \times n_u} \tag{8}$$

$$= \mathbf{B} \underbrace{\text{vec}((L^1 \mathbf{z}, \dots, L^p \mathbf{z})(t))}_{=: \zeta(t)} + \mathbf{U} \underbrace{\text{vec}((L^1 \mathbf{u}, \dots, L^q \mathbf{u})(t))}_{=: \mu(t)} \tag{9}$$

(9) uses block matrix notation  $\mathbf{B} = (\mathbf{B}_1, \dots, \mathbf{B}_p) \in \mathbb{R}^{r \times rp}$  and  $\mathbf{U} = (\mathbf{U}_1, \dots, \mathbf{U}_q) \in \mathbb{R}^{r \times n_u q}$ .

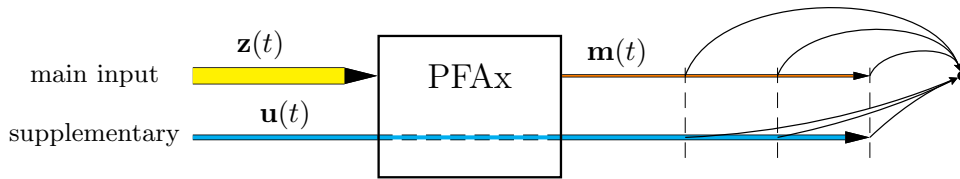


Figure 4: Illustration of PFAX. Components are selected to be well predictable if supplementary information is taken into account.

In (19) we will state the PFAX optimization problem in terms of (9), but that formulation requires a formula to express the prediction matrices  $\mathbf{B}$  and  $\mathbf{U}$  in terms of the extraction matrix  $\mathbf{A}_r$ . Matrix calculus allows us to compute the ideal prediction matrices for a given extraction  $\mathbf{A}_r$ :

$$\mathbf{B}(\mathbf{A}_r) := \left( \mathbf{A}_r^T \langle \mathbf{z}\zeta^T \rangle - \mathbf{U}(\mathbf{A}_r) \langle \mu\zeta^T \rangle \right) \underline{\mathbf{A}}_r \left( \underline{\mathbf{A}}_r^T \langle \zeta\zeta^T \rangle \underline{\mathbf{A}}_r \right)^{-1} \quad (10)$$

$$\mathbf{U}(\mathbf{A}_r) := \left( \mathbf{A}_r^T \langle \mathbf{z}\mu^T \rangle - \mathbf{B}(\mathbf{A}_r) \underline{\mathbf{A}}_r^T \langle \zeta\mu^T \rangle \right) \langle \mu\mu^T \rangle^{-1} \quad (11)$$

This uses the shortcut notation defined for any matrix  $\mathbf{M} \in \mathbb{R}^{n \times m}$ :

$$\underline{\mathbf{M}} := \mathbf{I}_{p,p} \otimes \mathbf{M} = \begin{pmatrix} \mathbf{M} & \mathbf{0} \\ & \ddots \\ \mathbf{0} & \mathbf{M} \end{pmatrix} \in \mathbb{R}^{np \times mp} \quad (12)$$

$p$  times  $\mathbf{M}$

Equations (10) and (11) are derived as follows. For a given  $\mathbf{A}_r$  the optimal  $\mathbf{B}$ ,  $\mathbf{U}$  must solve

$$\underset{\substack{\mathbf{B} \in \mathbb{R}^{r \times rp} \\ \mathbf{U} \in \mathbb{R}^{n_{\mathbf{u}} \times n_{\mathbf{u}g}}}}{\text{minimize}} \quad \langle \|\mathbf{A}_r^T \mathbf{z} - \mathbf{B} \underline{\mathbf{A}}_r^T \zeta - \mathbf{U} \mu\|^2 \rangle =: f(\mathbf{B}, \mathbf{U}) \quad (13)$$

Writing  $f(\mathbf{B}, \mathbf{U}) = \text{Tr} \left( \langle (\mathbf{A}_r^T \mathbf{z} - \mathbf{B} \underline{\mathbf{A}}_r^T \zeta - \mathbf{U} \mu) (\mathbf{A}_r^T \mathbf{z} - \mathbf{B} \underline{\mathbf{A}}_r^T \zeta - \mathbf{U} \mu)^T \rangle \right)$  we can expand  $f$  to

$$\begin{aligned} f(\mathbf{B}, \mathbf{U}) = \text{Tr} \left( \right. & \mathbf{A}_r^T \langle \mathbf{z}\mathbf{z}^T \rangle \mathbf{A}_r - \mathbf{A}_r^T \langle \mathbf{z}\zeta^T \rangle \underline{\mathbf{A}}_r \mathbf{B}^T - \mathbf{A}_r^T \langle \mathbf{z}\mu^T \rangle \mathbf{U}^T \\ & - \mathbf{B} \underline{\mathbf{A}}_r^T \langle \zeta\mathbf{z}^T \rangle \mathbf{A}_r + \mathbf{B} \underline{\mathbf{A}}_r^T \langle \zeta\zeta^T \rangle \underline{\mathbf{A}}_r \mathbf{B}^T + \mathbf{B} \underline{\mathbf{A}}_r^T \langle \zeta\mu^T \rangle \mathbf{U}^T \\ & \left. - \mathbf{U} \langle \mu\mathbf{z}^T \rangle \mathbf{A}_r + \mathbf{U} \langle \mu\zeta^T \rangle \underline{\mathbf{A}}_r \mathbf{B}^T + \mathbf{U} \langle \mu\mu^T \rangle \mathbf{U}^T \right) \end{aligned} \quad (14)$$

and set its matrix derivatives to zero:

$$\frac{\partial}{\partial \mathbf{B}} f(\mathbf{B}, \mathbf{U}) = -2\mathbf{A}_r^T \langle \mathbf{z}\zeta^T \rangle \underline{\mathbf{A}}_r + 2\mathbf{U} \langle \mu\zeta^T \rangle \underline{\mathbf{A}}_r + 2\mathbf{B} \underline{\mathbf{A}}_r^T \langle \zeta\zeta^T \rangle \underline{\mathbf{A}}_r \stackrel{!}{=} \mathbf{0} \quad (15)$$

$$\frac{\partial}{\partial \mathbf{U}} f(\mathbf{B}, \mathbf{U}) = -2\mathbf{A}_r^T \langle \mathbf{z}\mu^T \rangle + 2\mathbf{B} \underline{\mathbf{A}}_r^T \langle \zeta\mu^T \rangle + 2\mathbf{U} \langle \mu\mu^T \rangle \stackrel{!}{=} \mathbf{0} \quad (16)$$

Solving (15) for  $\mathbf{B}$  yields (10) and solving (16) for  $\mathbf{U}$  yields (11). In (10) and (11),  $\mathbf{B}(\mathbf{A}_r)$  and  $\mathbf{U}(\mathbf{A}_r)$  are defined implicitly. By inserting (11) into (10) and solving for  $\mathbf{B}(\mathbf{A}_r)$  we get the explicit formula

$$\mathbf{B}(\mathbf{A}_r) = \mathbf{A}_r^T \left( \langle \mathbf{z}\zeta^T \rangle - \langle \mathbf{z}\mu^T \rangle \langle \mu\mu^T \rangle^{-1} \langle \mu\zeta^T \rangle \right) \underline{\mathbf{A}}_r \left( \underline{\mathbf{A}}_r^T \left( \langle \zeta\zeta^T \rangle - \langle \zeta\mu^T \rangle \langle \mu\mu^T \rangle^{-1} \langle \mu\zeta^T \rangle \right) \underline{\mathbf{A}}_r \right)^{-1} \quad (17)$$

If  $\langle \mu\mu^T \rangle$  is not (cleanly) invertible due to very small or zero-valued eigenvalues, we recommend to project away the eigenspaces corresponding to eigenvalues below a critical threshold. These indicate redundancies in the signal and can therefore be dropped: In an eigenvalue decomposition of  $\langle \mu\mu^T \rangle$  replace eigenvalues below the threshold by 0 and invert the others. Use the resulting matrix as a proxy for  $\langle \mu\mu^T \rangle^{-1}$ . Proceed equivalently with other matrices where arising inversions are not computable due to near-zero-eigenvalues.

We define the ideal linear predictor  $\hat{\mathbf{z}}^{(0)}$  for the original signal without extraction, i.e.  $\mathbf{A}_r = \mathbf{I}$ :

$$\hat{\mathbf{z}}^{(0)}(t) := \mathbf{B}(\mathbf{I}) \zeta(t) + \mathbf{U}(\mathbf{I}) \mu(t) \quad (18)$$

and can now refine problem (4) to

$$\underset{\mathbf{A} \in \mathcal{O}(n)}{\text{minimize}} \quad \langle \|\mathbf{A}_r^T(\mathbf{z} - \hat{\mathbf{z}}^{(0)})\|^2 \rangle = \text{Tr} \left( \mathbf{A}_r^T \langle (\mathbf{z} - \hat{\mathbf{z}}^{(0)})(\mathbf{z} - \hat{\mathbf{z}}^{(0)})^T \rangle \mathbf{A}_r \right) \quad (19)$$

which can be solved by choosing  $\mathbf{A}$  such that it diagonalizes  $\langle (\mathbf{z} - \hat{\mathbf{z}}^{(0)})(\mathbf{z} - \hat{\mathbf{z}}^{(0)})^T \rangle$  and sorts the  $r$  smallest eigenvalues to the upper left. From this we obtain the prediction model by calculating  $\mathbf{B}_z(\mathbf{A}_r)$  and  $\mathbf{U}_z(\mathbf{A}_r)$ .

In [Richthofer and Wiskott, 2015], we proposed an iterated prediction as a heuristic method to better avoid overfitting. In [Richthofer and Wiskott, 2017] we extended this method to comply with supplementary information as follows. We define a matrix  $\mathbf{V}$  which implements the autoregressive model and predicts  $\zeta(t+1)$  from  $\zeta(t)$ :

$$\mathbf{V} := \left( \langle \zeta(t+1)\zeta^T \rangle - \mathbf{I}_{np,n} \mathbf{U}(\mathbf{I}) \langle \mu \zeta^T \rangle \right) \langle \zeta \zeta^T \rangle^{-1} \quad (20)$$

$$\hat{\mathbf{z}}^{(i)}(t) := \mathbf{B}(\mathbf{I}) \mathbf{V}^i \zeta(t-i) + \mathbf{I}_{np,n}^T \sum_{j=0}^i \mathbf{V}^j \mathbf{I}_{np,n} \mathbf{U}(\mathbf{I}) \mu(t-j) \quad (21)$$

Note that  $\hat{\mathbf{z}}^{(i)}$  is consistent with  $\hat{\mathbf{z}}^{(0)}$  in (18) for  $i=0$ . Based on  $\hat{\mathbf{z}}^{(i)}$  we proposed the optimization problem

$$\underset{\mathbf{A} \in \mathcal{O}(n)}{\text{minimize}} \quad \sum_{i=0}^k \langle \|\mathbf{A}_r^T(\mathbf{z} - \hat{\mathbf{z}}^{(i)})\|^2 \rangle = \text{Tr} \left( \mathbf{A}_r^T \sum_{i=0}^k \langle (\mathbf{z} - \hat{\mathbf{z}}^{(i)})(\mathbf{z} - \hat{\mathbf{z}}^{(i)})^T \rangle \mathbf{A}_r \right) \quad (22)$$

It can be solved by the same procedure as (19): Choose  $\mathbf{A}$  such that it diagonalizes  $\sum_{i=0}^k \langle (\mathbf{z} - \hat{\mathbf{z}}^{(i)})(\mathbf{z} - \hat{\mathbf{z}}^{(i)})^T \rangle$  and sort the lowest  $r$  eigenvalues to the upper left. Apply  $\mathbf{B}_z(\mathbf{A}_r)$  and  $\mathbf{U}_z(\mathbf{A}_r)$  to get the prediction matrices for the obtained extraction matrix.

## 2.2 Generating a control signal for local navigation

Considering an agent exploring an environment, we present the agent's perception as main input  $\mathbf{z}$  to PFAX and provide the preceding control command as supplementary information  $\mathbf{u}$ . This way the extracted predictable features will be a compact representation of perception aspects that are influenced by the control commands. We assume that the control signal is somehow generated during training phase, e.g. randomly within some constraints. After training phase, PFAX provides  $\mathbf{A}_r$ ,  $\mathbf{B}(\mathbf{A}_r)$  and  $\mathbf{U}(\mathbf{A}_r)$  and we want to reach a goal position  $\mathbf{m}^*$  in feature space, assuming that feature space is sufficiently representative to let us actually reach the associated goal in our environment. As explained earlier, we will apply SFA on top of PFAX, so in contrast to the original PFAX setting, we must consider an additional extraction matrix  $\mathbf{A}_{\text{SFA}}$ . This is a true generalization as  $\mathbf{A}_{\text{SFA}} = \mathbf{I}$  yields the original setting. Note that SFA also incorporates a mean shift, which is omitted here for simplicity and considering that PFAX output should be already mean free. Further more this would only result in a shift component for the cost function and is thus irrelevant for optimization. To calculate the ideal control command we minimize the least square distance between predicted features and goal features w.r.t. a preceding linear SFA step:

$$\underset{\mathbf{u}(t) \in \mathbb{R}^{n_u}}{\text{minimize}} \quad \|\mathbf{m}^* - \mathbf{A}_{\text{SFA}}^T (\mathbf{B}(\mathbf{A}_r) \mathbf{A}_r^T \zeta(t+1) - \mathbf{U}(\mathbf{A}_r) \mu(t+1))\|^2 \quad (23)$$

$$= \underbrace{\|\mathbf{m}^* - \mathbf{A}_{\text{SFA}}^T \left( \mathbf{B}(\mathbf{A}_r) \mathbf{A}_r^T \zeta(t+1) - \left( \sum_{j=2}^q \mathbf{U}_j(\mathbf{A}_r) \mathbf{u}(t-j+1) \right) \right) - \mathbf{A}_{\text{SFA}}^T \mathbf{U}_1 \mathbf{u}(t)\|}_{=: \mathbf{u}^* \in \mathbb{R}^r}^2 \quad (24)$$

$$= \|\mathbf{u}^* - \underbrace{\mathbf{A}_{\text{SFA}}^T \mathbf{U}_1}_{=: \tilde{\mathbf{U}}_1} \mathbf{u}(t)\|^2 \quad (25)$$

This problem is readily solved by choosing  $\mathbf{u}(t) := \tilde{\mathbf{U}}_1^{-1} \mathbf{u}^*$  (or  $\mathbf{u}(t) := (\tilde{\mathbf{U}}_1^T \tilde{\mathbf{U}}_1)^{-1} \tilde{\mathbf{U}}_1^T \mathbf{u}^*$ , if  $\tilde{\mathbf{U}}_1$  is not square or not invertible). Note that this would also minimize  $\|\mathbf{u}^* - \tilde{\mathbf{U}}_1 \mathbf{u}(t)\|$ . However, to incorporate constraints on  $\mathbf{u}$ , the squared distance is much friendlier for optimization.

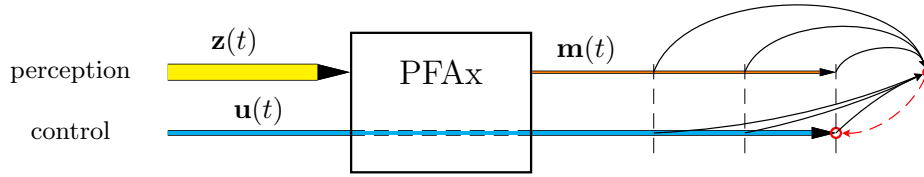


Figure 5: Illustration of controlling predictable features. The relation of control signal and prediction is inverted to obtain the control command that most likely yields the desired outcome.

Later we will model an agent moving with constant speed, which involves a normalized-length-constraint:

$$\underset{\substack{\mathbf{u}(t) \in \mathbb{R}^{n_u} \\ \|\mathbf{u}(t)\| = c}}{\text{minimize}} \quad \|\mathbf{u}^* - \tilde{\mathbf{U}}_1 \mathbf{u}(t)\|^2 \quad (26)$$

This is equivalent to the inhomogeneous eigenvalue problem

$$\tilde{\mathbf{U}}_1^T \tilde{\mathbf{U}}_1 \mathbf{u}(t) = \lambda \mathbf{u}(t) + \tilde{\mathbf{U}}_1^T \mathbf{u}^* \quad (27)$$

$$\|\mathbf{u}(t)\| = c \quad (28)$$

In [Mattheij and Söderlind, 1987] such problems are approached. One method from there can also be found in the appendix of [Richthofer and Wiskott, 2017]. In that work we provide some experiments indicating that this method is suitable for local navigation, but cannot readily navigate its way globally, e.g. around obstacles or through doors connecting multiple rooms. The following section extends this method such that it is capable of solving these kind of global navigation tasks.

### 3 From local to global navigation

To achieve global navigation, the Slow Feature Analysis algorithm (SFA) [Wiskott and Sejnowski, 2002] and its extension xSFA [Sprekeler et al., 2014] for blind source

separation play an important role. Especially the mathematical foundation of xSFA, which is grounded on the mathematical analysis of SFA in [Sprekeler and Wiskott, 2008] forms a key component for the navigation approach presented here. So we first comprehend the original SFA algorithm and then sketch its mathematical foundation, also stating key results of the theory that xSFA is based on. Finally we apply these results to our navigation setting, yielding an efficient algorithm for global navigation.

### 3.1 Recall SFA

Like PFA selects components by predictability, SFA selects them by slowness. As it was a central inspiration for PFA, SFA has some more similarities to it: The extraction is also optimized over a training phase  $\Omega_t$  and to avoid trivial/constant or repeated solutions, the output signals must have unit variance, zero mean and must be pairwise uncorrelated. We refer to the transformation as  $\mathbf{g}(\mathbf{x})$ , i.e. the  $i$ th extracted signal is given as  $\mathbf{y}_i(t) := \mathbf{g}_i(\mathbf{x}(t))$ . Note that these depend instantaneously on the input signal  $\mathbf{x}(t)$ , so SFA cannot just fulfill its goal by forming a lowpass filter. Operating on a general function space  $\mathcal{F}$  that fulfills the necessary mathematical requirements of integrability and differentiability, the SFA optimization problem can be formulated as follows:

$$\begin{aligned}
& \text{For } i \in \{1, \dots, r\} \\
& \underset{\mathbf{g}_i \in \mathcal{F}}{\text{minimize}} \quad \langle \dot{\mathbf{y}}_i^2 \rangle \\
& \text{subject to} \quad \langle \mathbf{y}_i \rangle = 0 \quad (\text{zero mean}) \\
& \quad \quad \quad \langle \mathbf{y}_i^2 \rangle = 1 \quad (\text{unit variance}) \\
& \quad \quad \quad \langle \mathbf{y}_i \mathbf{y}_j \rangle = 0 \quad \forall j < i \quad (\text{pairwise decorrelation})
\end{aligned} \tag{29}$$

Restricting  $\mathcal{F}$  to be finite dimensional, e.g. to the space of polynomials up to a certain degree, transforms (29) into an efficiently solvable eigenvalue problem. With the notation familiar from the PFA description in section 2.1, let  $\mathbf{h}$  denote a basis of  $\mathcal{F}$ . Then using  $\mathbf{h}$  as a nonlinear expansion on the input signal  $\mathbf{x}$ , extraction can be performed by linear transformation and projection. With an initial sphering, i.e. (2) and (3) from section 2.1 we can set  $\mathbf{g}_i(\mathbf{x}(t)) := \mathbf{a}_i^T \mathbf{z}(t)$  for extraction vectors  $\mathbf{a}_i \in \mathbb{R}^n$ . SFA then becomes the following linearized version of (29):

$$\begin{aligned}
& \text{For } i \in \{1, \dots, r\} \\
& \underset{\mathbf{a}_i \in \mathbb{R}^n}{\text{minimize}} \quad \mathbf{a}_i^T \langle \dot{\mathbf{z}} \dot{\mathbf{z}}^T \rangle \mathbf{a}_i \\
& \text{subject to} \quad \mathbf{a}_i^T \langle \mathbf{z} \rangle = 0 \quad (\text{zero mean}) \\
& \quad \quad \quad \mathbf{a}_i^T \langle \mathbf{z} \mathbf{z}^T \rangle \mathbf{a}_i = 1 \quad (\text{unit variance}) \\
& \quad \quad \quad \mathbf{a}_i^T \langle \mathbf{z} \mathbf{z}^T \rangle \mathbf{a}_j = 0 \quad \forall j < i \quad (\text{pairwise decorrelation})
\end{aligned} \tag{30}$$

Like in section 2.1, the sphering yields  $\langle \mathbf{z} \rangle = 0$  and  $\langle \mathbf{z} \mathbf{z}^T \rangle = \mathbf{I}$ , transforming the constraints to (5) and its associated matrix notation (6). Choosing  $\mathbf{a}_i$  as eigenvectors of  $\langle \dot{\mathbf{z}} \dot{\mathbf{z}}^T \rangle$ , corresponding to the eigenvalues in ascending order, yields  $\mathbf{A}_r$  solving (30) globally. [Wiskott and Sejnowski, 2002] describes this procedure in detail.

(30) is an important approximation (29) for practical solvability. To get an idea to what solutions (30) would converge if we increase the dimension of  $\mathbf{h}$ , we focus again on the SFA version

concerning an unrestricted function space  $\mathcal{F}$  and the ideal solutions one would expect there. More specifically, we focus on the scenario where  $\mathbf{x}(\mathbf{t})$  is composed of statistically independent sources  $\mathbf{s}_\alpha$ . [Sprekeler and Wiskott, 2008] and [Sprekeler et al., 2014] analyze this case, proposing xSFA as an extension to SFA that can identify such sources. We comprehend some theory and results:

Assuming that  $\mathbf{x}(\mathbf{t})$  is an ergodic process, SFA can be formulated in terms of the ensemble (i.e. the set of possible values of  $\mathbf{x}$  and  $\dot{\mathbf{x}}$ ) using the probability density  $p_{\mathbf{x},\dot{\mathbf{x}}}(\mathbf{x},\dot{\mathbf{x}})$ . The corresponding marginal and conditional densities are defined as  $p_{\mathbf{x}}(\mathbf{x}) := \int p_{\mathbf{x},\dot{\mathbf{x}}}(\mathbf{x},\dot{\mathbf{x}})d^n\dot{x}$  and  $p_{\dot{\mathbf{x}}|\mathbf{x}}(\dot{\mathbf{x}}|\mathbf{x}) := \frac{p_{\mathbf{x},\dot{\mathbf{x}}}(\mathbf{x},\dot{\mathbf{x}})}{p_{\mathbf{x}}(\mathbf{x})}$ . Further assuming that the ensemble averages  $\langle f(\mathbf{x},\dot{\mathbf{x}}) \rangle_{\mathbf{x},\dot{\mathbf{x}}} := \int p_{\mathbf{x},\dot{\mathbf{x}}}(\mathbf{x},\dot{\mathbf{x}})f(\mathbf{x},\dot{\mathbf{x}})d^n\mathbf{x}d^n\dot{x}$ ,  $\langle f(\mathbf{x}) \rangle_{\mathbf{x}} := \int p_{\mathbf{x}}(\mathbf{x})f(\mathbf{x})d^n\mathbf{x}$  and  $\langle f(\mathbf{x},\dot{\mathbf{x}}) \rangle_{\dot{\mathbf{x}}|\mathbf{x}}(\mathbf{x}) := \int p_{\dot{\mathbf{x}}|\mathbf{x}}(\dot{\mathbf{x}}|\mathbf{x})f(\mathbf{x},\dot{\mathbf{x}})d^n\dot{x}$  all exist and using the chain rule, the SFA optimization problem can be stated in terms of the ensemble as well:

For  $i \in \{1, \dots, r\}$

$$\begin{aligned} & \underset{\mathbf{g}_i \in \mathcal{F}}{\text{minimize}} && \sum_{\gamma,\nu} \left\langle \partial_\gamma \mathbf{g}_i(\mathbf{x}) \langle \dot{\mathbf{x}}_\gamma \dot{\mathbf{x}}_\nu \rangle_{\dot{\mathbf{x}}|\mathbf{x}} \partial_\nu \mathbf{g}_i(\mathbf{x}) \right\rangle_{\mathbf{x}} \\ & \text{subject to} && \langle \mathbf{g}_i(\mathbf{x}) \rangle_{\mathbf{x}} = 0 && \text{(zero mean)} \\ & && \langle \mathbf{g}_i^2(\mathbf{x}) \rangle_{\mathbf{x}} = 1 && \text{(unit variance)} \\ & && \langle \mathbf{g}_i(\mathbf{x}) \mathbf{g}_j(\mathbf{x}) \rangle_{\mathbf{x}} = 0 \quad \forall j < i && \text{(pairwise decorrelation)} \end{aligned} \quad (31)$$

A key result from [Sprekeler and Wiskott, 2008] is that the ideal solutions for SFA on an unrestricted function space can be found by solving the following eigenvalue equation given the partial differential operator  $\mathcal{D} := -\frac{1}{p_{\mathbf{x}}(\mathbf{x})} \sum_{\gamma,\nu} \partial_\gamma p_{\mathbf{x}}(\mathbf{x}) \langle \dot{\mathbf{x}}_\gamma \dot{\mathbf{x}}_\nu \rangle_{\dot{\mathbf{x}}|\mathbf{x}}(\mathbf{x}) \partial_\nu$ :

$$\mathcal{D} \mathbf{g}_i(\mathbf{x}) = \lambda_i \mathbf{g}_i(\mathbf{x}) \quad (32)$$

under the von Neumann boundary conditions

$$\sum_{\gamma,\nu} n_\gamma(\mathbf{x}) p_{\mathbf{x}}(\mathbf{x}) \langle \dot{\mathbf{x}}_\gamma \dot{\mathbf{x}}_\nu \rangle_{\dot{\mathbf{x}}|\mathbf{x}}(\mathbf{x}) \partial_\nu \mathbf{g}_i(\mathbf{x}) \quad (33)$$

where  $n_\gamma(\mathbf{x})$  is the  $\gamma$ th component of the normal vector at the boundary point  $\mathbf{x}$ . Assuming the input signal  $\mathbf{x}(t)$  is composed of statistically independent sources  $\mathbf{s}_\alpha$  for  $\alpha \in \{1, \dots, S\}$ , this result can be formulated in terms of the sources. Because of statistical independence we have  $p_{\mathbf{s},\dot{\mathbf{s}}}(\mathbf{s},\dot{\mathbf{s}}) = \prod_\alpha p_{\mathbf{s}_\alpha,\dot{\mathbf{s}}_\alpha}(\mathbf{s}_\alpha,\dot{\mathbf{s}}_\alpha)$ ,  $p_{\mathbf{s}}(\mathbf{s}) = \prod_\alpha p_{\mathbf{s}_\alpha}(\mathbf{s}_\alpha)$  and  $\langle \dot{\mathbf{s}}_\alpha \dot{\mathbf{s}}_\beta \rangle_{\dot{\mathbf{s}}|\mathbf{s}}(\mathbf{s}) = \delta_{\alpha\beta} \langle \dot{\mathbf{s}}_\alpha^2 \rangle_{\dot{\mathbf{s}}_\alpha|\mathbf{s}_\alpha}(\mathbf{s}_\alpha)$ .  $\mathcal{D}(\mathbf{s})$  can be decomposed as

$$\mathcal{D}(\mathbf{s}) = \sum_\alpha \mathcal{D}_\alpha(\mathbf{s}_\alpha) \quad (34)$$

Regarding this decomposition, (32) and (33) can be reformulated such that, with an additional normalization constraint, the following equations formulate SFA in terms of the sources:

$$\mathcal{D}_\alpha \mathbf{g}_{\alpha i} = \lambda_{\alpha i} \mathbf{g}_{\alpha i} \quad (35)$$

$$p_\alpha \langle \dot{\mathbf{s}}_\alpha^2 \rangle_{\dot{\mathbf{s}}_\alpha|\mathbf{s}_\alpha} \partial_\alpha \mathbf{g}_{\alpha i} = 0 \quad \text{on the boundary} \quad (36)$$

$$\langle \mathbf{g}_{\alpha i}^2 \rangle_{\mathbf{s}_\alpha} = 1 \quad (37)$$

*Theorem 2* in [Sprekeler and Wiskott, 2008] / *Theorem 1* in [Sprekeler et al., 2014] states that the solutions of (32) are composed from solutions of (35):

$$\mathbf{g}_i(\mathbf{s}) = \prod_{\alpha} \mathbf{g}_{\alpha i_{\alpha}}(\mathbf{s}_{\alpha}) \quad (38)$$

$$\lambda_i = \sum_{\alpha} \lambda_{\alpha i_{\alpha}} \quad (39)$$

with  $\mathbf{i} = (i_1, \dots, i_S) \in \mathbb{N}^S$  denoting a multi index to select the right combination of sources. Choosing the  $r$  smallest eigenvalues  $\lambda_i$  yields the  $r$  slowest output signals.

Another crucial result from [Sprekeler and Wiskott, 2008] and [Sprekeler et al., 2014] states monotonicity of each first harmonic  $\mathbf{g}_{\alpha 1}(\mathbf{s}_{\alpha})$  w.r.t.  $\mathbf{s}_{\alpha}$ . For later reference we denote this result as Lemma 1 and comprehend the proof. We extend the lemma by remarking that it does not require  $p_{\alpha}$  to be a probability distribution. It rather works for any strictly positive weighting function. We will make use of this fact later on.

**Lemma 1**

*If  $\mathbf{s}$  consists of statistically independent components  $\mathbf{s}_{\alpha}$  like introduced above, then for each source  $\mathbf{s}_{\alpha}$  the first harmonic  $\mathbf{g}_{\alpha 1}(\mathbf{s}_{\alpha})$  is a monotonic signal of the source  $\mathbf{s}_{\alpha}$ . This also holds if the distribution  $p_{\alpha}$  of  $\mathbf{s}_{\alpha}$  is not a probability distribution, but any strictly positive weighting function.*

*Proof.* In standard form of a Sturm-Liouville problem and assuming that  $\mathbf{s}_{\alpha}$  maps to the interval  $I_{\alpha} = [a_{\alpha}, b_{\alpha}]$ , (35)/(36) are stated as

$$\partial_{\alpha} p_{\alpha} \langle \dot{\mathbf{s}}_{\alpha}^2 \rangle_{\dot{\mathbf{s}}_{\alpha} | \mathbf{s}_{\alpha}} \partial_{\alpha} \mathbf{g}_{\alpha i} + \lambda_{\alpha i} p_{\alpha} \mathbf{g}_{\alpha i} = 0 \quad (40)$$

$$p_{\alpha} \langle \dot{\mathbf{s}}_{\alpha}^2 \rangle_{\dot{\mathbf{s}}_{\alpha} | \mathbf{s}_{\alpha}} \partial_{\alpha} \mathbf{g}_{\alpha i} = 0 \quad \forall \mathbf{s}_{\alpha} \in \{a_{\alpha}, b_{\alpha}\} \quad (41)$$

With Sturm-Liouville theory stating that  $\mathbf{g}_{\alpha 1}$  has only one zero  $\xi \in (a_{\alpha}, b_{\alpha})$  we assume that without loss of generality  $\mathbf{g}_{\alpha 1} < 0$  for  $\mathbf{s}_{\alpha} < \xi$  and  $\mathbf{g}_{\alpha 1} > 0$  for  $\mathbf{s}_{\alpha} > \xi$ .

$$(40) \Rightarrow \partial_{\alpha} p_{\alpha} \langle \dot{\mathbf{s}}_{\alpha}^2 \rangle_{\dot{\mathbf{s}}_{\alpha} | \mathbf{s}_{\alpha}} \partial_{\alpha} \mathbf{g}_{\alpha 1} = - \underbrace{\lambda_{\alpha 1} p_{\alpha}}_{>0} \mathbf{g}_{\alpha 1} < 0 \quad \forall \mathbf{s}_{\alpha} > \xi \quad (42)$$

$$\Rightarrow p_{\alpha} \langle \dot{\mathbf{s}}_{\alpha}^2 \rangle_{\dot{\mathbf{s}}_{\alpha} | \mathbf{s}_{\alpha}} \partial_{\alpha} \mathbf{g}_{\alpha 1} \text{ monotonically increasing on } (\xi, b_{\alpha}] \quad (43)$$

$$\stackrel{(41)}{\Rightarrow} \underbrace{p_{\alpha} \langle \dot{\mathbf{s}}_{\alpha}^2 \rangle_{\dot{\mathbf{s}}_{\alpha} | \mathbf{s}_{\alpha}}}_{>0} \partial_{\alpha} \mathbf{g}_{\alpha 1} > 0 \text{ on } (\xi, b_{\alpha}) \quad (44)$$

$$\Rightarrow \partial_{\alpha} \mathbf{g}_{\alpha 1} > 0 \text{ on } (\xi, b_{\alpha}) \quad (45)$$

$$\Leftrightarrow \mathbf{g}_{\alpha 1} \text{ monotonically increasing on } (\xi, b_{\alpha}] \quad (46)$$

Equivalently it holds that  $\mathbf{g}_{\alpha 1}$  is monotonically increasing on  $[a_{\alpha}, \xi)$ , implying that  $\mathbf{g}_{\alpha 1}$  is monotonically increasing on the whole interval  $I_{\alpha}$ .

The calculation above does not require  $p_{\alpha}$  to be a probability distribution, but only to be a strictly positive weighting function.  $\square$

We list some additional important results from [Sprekeler and Wiskott, 2008] and [Sprekeler et al., 2014]:

- If the sources are normally distributed, i.e.  $p_\alpha(\mathbf{s}_\alpha) = \frac{1}{\sqrt{2\pi}} e^{-\frac{1}{2}\mathbf{s}_\alpha^2}$ , then  $\langle \dot{\mathbf{s}}_\alpha^2 \rangle_{\dot{\mathbf{s}}_\alpha|\mathbf{s}_\alpha}$  is constant and the Hermite polynomials  $H_i$  yield the solutions  $\mathbf{g}_{\alpha i}(\mathbf{s}_\alpha) = \frac{1}{\sqrt{2^i i!}} H_i(\frac{\mathbf{s}_\alpha}{\sqrt{2}})$  with  $\lambda_{\alpha i} = \frac{i}{\langle \dot{\mathbf{s}}_\alpha^2 \rangle_{\dot{\mathbf{s}}_\alpha|\mathbf{s}_\alpha}}$ .
- If the sources are uniformly distributed, then  $\langle \dot{\mathbf{s}}_\alpha^2 \rangle_{\dot{\mathbf{s}}_\alpha|\mathbf{s}_\alpha}$  is constant and the solutions are given by Sturm-Liouville theory as harmonic oscillations  $\mathbf{g}_{\alpha i}(\mathbf{s}_\alpha) = \sqrt{2} \cos(i\pi \frac{\mathbf{s}_\alpha}{L_\alpha})$  with  $\lambda_{\alpha i} = \langle \dot{\mathbf{s}}_\alpha^2 \rangle_{\dot{\mathbf{s}}_\alpha|\mathbf{s}_\alpha} (\frac{\pi}{L_\alpha} i)^2$ , assuming that  $\mathbf{s}_\alpha$  takes values in the interval  $[0, L_\alpha]$ . Therefore one refers to  $\mathbf{g}_{\alpha i}$  as the  $i$ th harmonic of the source  $\mathbf{s}_\alpha$ . Note that in this case, all higher harmonics can be calculated from the first harmonic using the Chebyshev polynomials  $T_i$ :  $\mathbf{g}_{\alpha i} = T_i(\mathbf{g}_{\alpha 1})$
- The slowest signal found by SFA is plainly the first harmonic  $\mathbf{g}_{\alpha 1}$  of the slowest source. This result is a corner stone of xSFA as it allows to clean subsequent signals from the first source. Iterating this procedure finally yields all sources.
- (38) implies that each output component  $\mathbf{g}_i$  of SFA is a product of harmonics  $\mathbf{g}_{\alpha i}$  of earlier obtained sources.

### 3.1.1 SFA harmonics illustrated on a 1D random walk

To illustrate the role of harmonics for one specific source, we demonstrate the theory on a simple 1D random walk on the interval  $[0, 100]$ . An agent starts at position 50 and each step is chosen by a uniform distribution over the interval  $[-\frac{1}{2}, \frac{1}{2}]$ . Steps exceeding the left or right boundary are simply cut off.

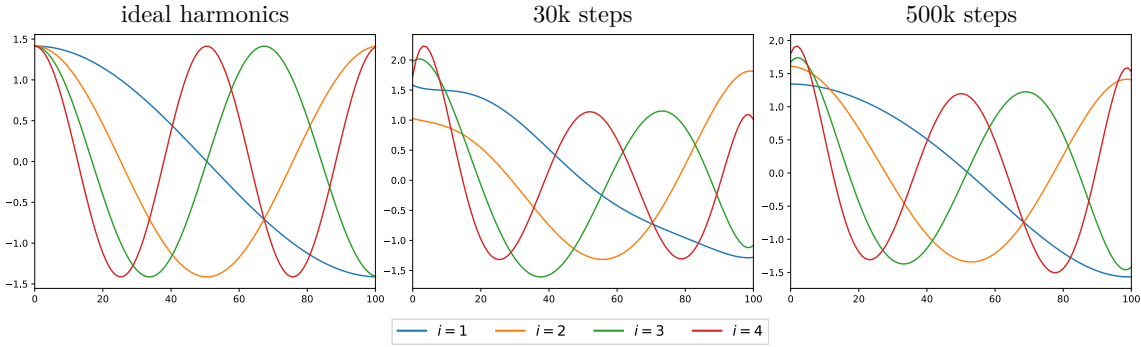


Figure 6: Illustration of the first four harmonics. The ideal harmonics predicted by the theory (left) and harmonics extracted by SFA from a 1D random walk on  $[0, 100]$ , i.e. from a single source. A longer random walk (right) approximates uniform distribution – and thus the ideal harmonics – better than a shorter (middle).

We provide the plain position as input to SFA, using monomials up to the sixth degree as expansion. We extract the first four harmonics and compare them to those predicted by the theory. Although a 1D random walk usually yields a normal distribution around the starting point, for long training phases and due to the boundaries, the distribution actually approaches uniformity with some bias near the boundary. Figure 6 illustrates this effect, comparing a shorter



walk consisting of 30000 steps with a longer walk consisting of 500000 steps. Another notable effect is that lower harmonics are usually extracted cleaner than higher harmonics, which is due to the limited monomial expansion. Further note that the monotonicity of the first harmonic is mostly preserved even if the harmonic itself was not cleanly extracted. The algorithm presented in this paper benefits from this effect as it mainly exploits the first harmonic of each source and especially its monotonicity.

## 3.2 xSFA on manifolds

For the blind source separation setting in [Sprekeler et al., 2014] it is assumed that the input is composed from statistically independent sources. This assumption is not necessarily appropriate for the setting studied in this paper. A closer fit can be found in [Franzius et al., 2007] where the agent’s state space, denoted *configuration space*  $\mathcal{V}$ , is considered a manifold embedded in the sensor space that yields the data subject of study. In this section we extend xSFA theory from [Sprekeler et al., 2014] to such a manifold setting and establish a geometrical characterization of the solutions in terms of potential, monotonicity, geodesics and manifold representation. These results motivate the navigation algorithm proposed in section 3.3.

### 3.2.1 Slowest features are monotonic flows on the state space

Lemma 1 shows monotonicity with respect to the slowest source, but does not characterize the source itself in context of the state space  $\mathcal{V}$ . We can show that under certain assumptions, the slowest features actually correspond to monotonic flows across  $\mathcal{V}$ . In the notation from [Franzius et al., 2007] the sources in terms of xSFA are the agent’s possible configurations  $\mathbf{s} \in \mathcal{V}$ . For a fully observable environment and a sufficiently rich sensor, each sensor input value  $\mathbf{x}(t)$  can be identified with a value  $\mathbf{s} = \psi(\mathbf{x}) \in \mathcal{V}$  such that  $\psi$  is an bijective map. Each output component  $\mathbf{g}_i$  of xSFA is a scalar field on  $\mathcal{V}$ , mapping  $\mathbf{s}$  to a real number. We can assume  $\mathbf{g}_i$  is bounded so it actually maps to an interval  $I_i = [\min_i, \max_i]$ , i.e.  $\mathbf{g}_i: \mathcal{V} \rightarrow I_i$ . Let  $\mathbf{g}_i^{-1}(\theta)$  denote the fiber of  $\theta \in I_i$ . These are also known as level sets or equipotential sets. With a plain  $I$  we denote the unit interval  $I := [0, 1]$ . Mapping from  $\mathcal{V}$  to  $\mathbb{R}$ ,  $\mathbf{g}_i$  usually performs a dimensionality reduction, unless  $\mathcal{V} \subset \mathbb{R}$ . It proves advantageous to study the layout of this reduction, i.e. of the fibers of  $\mathbf{g}_i$  separately from its value. We achieve this separation by splitting

$$\mathbf{g}_i(\mathbf{s}) =: \tilde{\mathbf{g}}_i(t_i(\mathbf{s})) \quad \text{with} \quad \tilde{\mathbf{g}}_i: I \rightarrow I_i, \quad t_i: \mathcal{V} \rightarrow I \quad (47)$$

$t_i$  is some scalar field on  $\mathcal{V}$  realizing the level sets of  $\mathbf{g}_i$ , while  $\tilde{\mathbf{g}}_i$  is a real-valued function realizing the value of  $\mathbf{g}_i$  on top of  $t_i$ . We refer to  $t_i$  as the coordinate function of  $\mathbf{g}_i$ , because it defines a one-dimensional coordinate for  $\tilde{\mathbf{g}}_i$  on  $\mathcal{V}$ . If  $\tilde{\mathbf{g}}_i$  is injective,  $t_i$  must have the same level sets as  $\mathbf{g}_i$ . Otherwise  $t_i$  assigns distinct values to separate connectivity components of level sets of  $\mathbf{g}_i$  whenever such components are induced by  $\tilde{\mathbf{g}}_i$  being non-injective. Also note that  $t_i$  can differ from  $\mathbf{g}_i$  in velocity and that  $t_i$  only underlies Von Neumann boundary conditions where its fibers hit the boundary orthogonally. Note that the choice of  $t_i$  is not unique. E.g. every composition of  $t_i$  with a bijective function yields another valid  $t_i$ . This gives us the freedom to assume additional properties on  $t_i$ , most notably uniform velocity of its integral curves.

#### Theorem 1

Let  $\mathbf{g}_i$  be the solution components of xSFA. For every  $\tilde{\mathbf{g}}_i, t_i$  like defined in (47) with  $\mathbf{g}_i = \tilde{\mathbf{g}}_i \circ t_i$

the following holds. Let  $\varphi_{\mathbf{a},\mathbf{b}}: I \rightarrow \mathcal{V}$  be an integral curve of  $\nabla t_i$  from  $\mathbf{a} \in \mathbf{g}_i^{-1}(\min_i)$  to  $\mathbf{b} \in \mathbf{g}_i^{-1}(\max_i)$  or contrary. Then it runs through  $\mathcal{V}$  strictly monotonically w.r.t.  $\mathbf{g}_i$ , i.e.  $\mathbf{g}_i \circ \varphi_{\mathbf{a},\mathbf{b}}$  is a strictly monotonic function.

Intuitively this means that  $\mathbf{g}_i$  has no local extrema or bumps spatially “between” its minimal and maximal level sets. It does not rule out local extrema completely but they must be somewhat isolated from the main flow, e.g. in another branch of  $\mathcal{V}$ . Theorem 1 is the first step of characterizing  $\mathbf{g}_i$  to consist of monotonic flows that bridge the potential spanned by  $\mathbf{g}_i^{-1}(\min_i)$  and  $\mathbf{g}_i^{-1}(\max_i)$  in the slowest possible fashion, or in – terms of potential theory – with minimal energy. Note that due to super position principle,  $\mathbf{g}_i$  can consist of multiple overlapping flows of this kind. Then it can happen that  $\mathbf{g}_i^{-1}(\min_i)$  or  $\mathbf{g}_i^{-1}(\max_i)$  is not connected.

*Proof.* Let  $R_i$  be the set of integral curves  $\varphi(\theta)$  of  $\nabla t_i$ . We assume that  $\mathcal{V}$  provides sufficient structure to define integration over  $R_i$ , e.g.  $\mathcal{V}$  could be a Riemannian manifold. With  $dV$  we denote integration by volume over  $\mathcal{V}$  and with  $dS$  we denote integration by volume over  $R_i$  in the sense that  $R_i$  is a hyper surface in  $\mathcal{V}$ . With  $D$  denoting the Jacobi matrix, we can write the SFA optimization criterion as follows (c.f. optimization problem 2 in [Franzius et al., 2007]):

$$\langle (\nabla \mathbf{g}_i(\mathbf{s}) \dot{\mathbf{s}})^2 \rangle_{\mathbf{s}, \dot{\mathbf{s}}} = \int_{\mathcal{V}} p_{\mathbf{s}}(\mathbf{s}) (D\mathbf{g}_i)(\mathbf{s}) \underbrace{\langle \dot{\mathbf{s}} \dot{\mathbf{s}}^T \rangle_{\dot{\mathbf{s}}|\mathbf{s}}}_{=: \mathbf{K}(\mathbf{s})} (D\mathbf{g}_i)^T(\mathbf{s}) dV \quad (48)$$

$$= \int_{\mathcal{V}} p_{\mathbf{s}}(\mathbf{s}) (D\tilde{\mathbf{g}}_i)^2 (Dt_i)\mathbf{K}(\mathbf{s})(Dt_i)^T dV \quad (49)$$

$$= \int_{R_i} p_{\varphi}(\varphi) \int_I \underbrace{p_{\theta|\varphi}(\theta|\varphi) \rho(\theta)}_{=: \tilde{p}(\theta)} (D\tilde{\mathbf{g}}_i)^2 \underbrace{(Dt_i)(\varphi(\theta))\mathbf{K}(\mathbf{s})(Dt_i)^T(\varphi(\theta))}_{=: \mathbf{K}_i(\theta)} d\theta dS \quad (50)$$

Here,  $\rho$  denotes the volume element regarding  $\theta$ . Since  $\mathbf{K}(\mathbf{s})$  can be interpreted as the empirically measured inverse metric tensor of  $\mathcal{V}$ , we have  $\rho(\theta) = \sqrt{|\det((\nabla\varphi)^T(\theta)\mathbf{G}(\mathbf{s})(\nabla\varphi)(\theta))|}$  with  $\mathbf{G}(\mathbf{s}) = \mathbf{K}^{-1}(\mathbf{s})$ .

We transform the unit variance constraint in a similar way:

$$\langle \mathbf{g}_i^2(\mathbf{s}) \rangle_{\mathbf{s}} = \int_{\mathcal{V}} p_{\mathbf{s}}(\mathbf{s}) \mathbf{g}_i^2(\mathbf{s}) dV = \int_{\mathcal{V}} p_{\mathbf{s}}(\mathbf{s}) \tilde{\mathbf{g}}_i^2(t_i(\mathbf{s})) dV \quad (51)$$

$$= \int_{R_i} p_{\varphi}(\varphi) \int_I p_{\theta|\varphi}(\theta|\varphi) \rho(\theta) \tilde{\mathbf{g}}_i^2(t_i(\varphi(\theta))) d\theta dS \quad (52)$$

$$= \int_{R_i} p_{\varphi}(\varphi) \int_I \underbrace{\tilde{p}(\theta) \tilde{\mathbf{g}}_i^2(t_i(\varphi(\theta)))}_{=: v_{\varphi} > 0} d\theta dS \quad (53)$$

A valid solution  $\mathbf{g}_i$  must yield

$$\int_{R_i} p_{\varphi}(\varphi) v_{\varphi} dS = 1 \quad (54)$$

Since  $p_\varphi(\varphi), v_\varphi > 0$ , every  $\varphi \in R_i$  contributes a positive quantity to the overall unit variance. Let  $v_\varphi^*$  be the family of quantities that yield the slowest signal  $\mathbf{g}_1$ . The distribution of variance across  $R_1$  is the only tread-off between the integral curves forming  $t_1$ , so we can conclude that for each  $\varphi \in R_1$ ,  $\mathbf{g}_1 \circ \varphi$  must be the solution of an optimization problem of the following form:

$$\begin{aligned} & \underset{\mathbf{g}_1 \in \mathcal{F}}{\text{minimize}} && \int_I \tilde{p}(\theta) (D\tilde{\mathbf{g}}_1)^2 \mathbf{K}_1(\theta) d\theta \\ & \text{subject to} && \int_I \tilde{p}(\theta) \tilde{\mathbf{g}}_1^2(t_1(\varphi(\theta))) d\theta = v_\varphi^* \end{aligned} \quad (55)$$

The crucial advantage of having  $t_i$  split off is that now  $\mathbf{K}_i(\theta)$  is scalar-valued. So (55) is an ordinary SFA optimization problem defined on the interval  $I$ . It is a bit special, because the variance is not normalized to 1 but to  $v_\varphi^*$  and  $\tilde{p}(\theta)$  is not a probability distribution but a general strictly positive weight function. However, these are just scaling issues and the mathematical theory of SFA solutions is still applicable. The underlying space  $I$  is one-dimensional, so it can only involve a single source, which must have coordinate character on  $I$ , i.e. be bijective and continuous, thus monotonic. Since a single source is always statistically independent, we can apply Lemma 1 and find that for every  $\varphi \in R_1$  the slowest solution  $\tilde{\mathbf{g}}_1 \circ t_1 \circ \varphi$  must be a strictly monotonic function on the interior of  $I$ , denoted  $I \setminus \partial I$ . Therefore we have for  $\theta \in I \setminus \partial I$ :

$$D(\tilde{\mathbf{g}}_1 \circ t_1 \circ \varphi) = D\tilde{\mathbf{g}}_1 Dt_1 D\varphi \neq \mathbf{0} \quad (56)$$

$\theta \in \partial I$  corresponds to  $\varphi(\theta) \in \mathbf{g}_i^{-1}(\min_i)$  or  $\varphi(\theta) \in \mathbf{g}_i^{-1}(\max_i)$ . For  $\theta \in I \setminus \partial I$  it follows that  $D\mathbf{g}_1, D\tilde{\mathbf{g}}_1, Dt_1, D\varphi$  are each non-zero and  $Dt_1 \not\perp D\varphi$ . This readily proves theorem 1 for  $i = 1$ .

To extend the proof to  $i > 1$  we need to recall how xSFA operates. After  $\mathbf{g}_1$  is extracted, in an idealized xSFA the data is projected onto a space orthogonal to the space of continuous functions of  $\mathbf{g}_1$ . We can think of an infinite sequence of monomials of  $\mathbf{g}_1$  as a basis of this space. Essentially the projection implies

$$\langle \mathbf{g}_1^k \mathbf{g}_2 \rangle_{\mathbf{s}} = 0 \quad \forall k \in \mathbb{N} \quad (57)$$

and consequently that

$$\langle \tilde{\mathbf{g}}_1^k(t_1) \tilde{\mathbf{g}}_2(t_2) \rangle_{\mathbf{s}} = 0 \quad \forall k \in \mathbb{N} \quad (58)$$

Since  $\tilde{\mathbf{g}}_1$  is monotonic we can build a Taylor expansion of the identity function from  $\tilde{\mathbf{g}}_1^k(t_1)$ , yielding that already the coordinate  $t_1$  is orthogonal to  $\tilde{\mathbf{g}}_2$ :

$$\langle t_1 \tilde{\mathbf{g}}_2(t_2) \rangle_{\mathbf{s}} = 0 \quad \forall k \in \mathbb{N} \quad (59)$$

Therefore we can express this constraint on coordinate level and restrict  $t_2$  to fulfill

$$\langle t_1 t_2 \rangle_{\mathbf{s}} = 0 \quad \forall k \in \mathbb{N} \quad (60)$$

which imposes no further constraint on  $\tilde{\mathbf{g}}_2$ . That means, the decorrelation constraint for  $i > j$  in xSFA sense only affects  $t_i$ , rather than  $\mathbf{g}_i$ , and is encoded in  $\mathbf{K}_i(\varphi)$ . So we can apply (55) with  $i > 1$  and equation (56), follows.  $\square$

Our next theorem characterizes the ideal spatial location of  $\mathbf{g}_i^{-1}(\min_i)$  and  $\mathbf{g}_i^{-1}(\max_i)$  in  $\mathcal{V}$ . Before we state it, we need to elaborate a bit on notation.

In the above proof of theorem 1 it was mentioned that the matrix  $\mathbf{K}(\mathbf{s})$  is related to a metric tensor on  $\mathcal{V}$ . Since it acts on the gradient of  $\mathbf{g}_i$  it must correspond to the dual metric tensor on  $\mathcal{V}$ . That means, when we measure arc length in  $\mathcal{V}$  we must do this w.r.t. a metric tensor  $\mathbf{G}(\mathbf{s}) = \mathbf{K}(\mathbf{s})^{-1}$ . With  $\nabla^\perp$  we denote the Jacobi matrix projected onto the space orthogonal to the gradient. This is also called the *skew gradient*. We can write

$$\det(D\varphi) = \sqrt{\det((D\varphi)^T(D\varphi))} = \sqrt{\det((\nabla\varphi)^T(\nabla\varphi)) \det((\nabla^\perp\varphi)^T(\nabla^\perp\varphi))} = |\nabla\varphi|g(\nabla^\perp\varphi) \quad (61)$$

For a custom metric tensor we have the volume element  $\rho(\varphi) = |\nabla\varphi|_{\mathbf{G}}g(\nabla^\perp\varphi)$  with  $g(\mathbf{V}) = \sqrt{|\det(\mathbf{V}^T\mathbf{G}(\mathbf{s})\mathbf{V})|}$  respectively. We are now ready to state theorem 2:

**Theorem 2**

Let  $\mathbf{g}_i$  be the solution components of xSFA. Let  $\tilde{\mathbf{g}}_i, t_i$  be like defined in (47), i.e.  $\mathbf{g}_i = \tilde{\mathbf{g}}_i \circ t_i$ . Let  $\varphi \in R_i$  be the integral curves of  $\nabla t_i$  running from  $\mathbf{g}_i^{-1}(\min_i)$  to  $\mathbf{g}_i^{-1}(\max_i)$ . If  $R_i$  is globally parameterizable by some appropriate parameter space  $\mathbf{I}_{R_i}$ , i.e. for  $\mathbf{r} \in \mathbf{I}_{R_i}$  let  $\varphi_{\mathbf{r}}$  denote a parametrization of  $R_i$ . If  $t_i$  can be chosen such that every  $\varphi \in R_i$  is parametrized by arc length, i.e.

$$\forall \mathbf{r} \in \mathbf{I}_{R_i}: \quad |(\nabla t_i)(\varphi_{\mathbf{r}}(\theta))|_{\mathbf{G}} = C_{\mathbf{r}} \quad (62)$$

where  $C_{\mathbf{r}}$  denotes a constant for a given  $\mathbf{r}$ , and such that  $|\nabla\varphi_{\mathbf{r}}(\theta)|_{\mathbf{G}}$  and  $g(\nabla^\perp\varphi_{\mathbf{r}})$  induce independent coordinates on  $R_i$  in the sense that for a fixed  $\theta$

$$\int_{\mathbf{I}_{R_i}} p_{\mathbf{s}}(\varphi_{\mathbf{r}}(\theta))|\nabla\varphi_{\mathbf{r}}(\theta)|_{\mathbf{G}}g(\nabla^\perp\varphi_{\mathbf{r}}) d\mathbf{r} = \int_{\mathbf{I}_{R_i}} |\nabla\varphi_{\mathbf{r}}(\theta)|_{\mathbf{G}} d\mathbf{r} \int_{\mathbf{I}_{R_i}} p_{\mathbf{s}}(\varphi_{\mathbf{r}}(\theta))g(\nabla^\perp\varphi_{\mathbf{r}}(\theta)) d\mathbf{r} \quad (63)$$

Then, for  $i = 1$  the sets  $\mathbf{g}_i^{-1}(\min_i)$  and  $\mathbf{g}_i^{-1}(\max_i)$  are located in  $\mathcal{V}$  such that all  $\varphi \in R_i$

- have lengths as equal as possible
- are in average as long as possible
- are as close as possible to geodesics
- cover a volume of  $\mathcal{V}$  as large as possible

For  $i > 1$  the named goals apply subject to the coordinate  $t_i$  being uncorrelated to coordinates  $t_j$  with  $j < i$ .

It should be possible to translate the requirement of a global parametrization of  $R_i$  to the setting of  $R_i$  spanning multiple coordinate charts. This is a primarily technical challenge and is subject of future work.

We can say a bit about the geometrical implications of (62) and (63). If  $\mathbf{g}_i$  has connected level sets, due to continuity it should be possible to scale every streamline of  $t_i$  intrinsically such that it fulfills (62). If the same can be applied to the level sets such that each level set is parameterized independently from  $\mathbf{r}$ , then  $g(\nabla^\perp\varphi_{\mathbf{r}}(\theta))$  depends only on  $\theta$  and (63) is readily fulfilled. Further note that under some regularity assumptions on  $\mathcal{V}$ , especially on  $\partial\mathcal{V}$ ,  $t_i$  can be chosen as a harmonic function. Here the terminus should not be confused with harmonics in other sections of this work, referring to harmonic oscillations. Instead it refers to harmonic functions from potential theory, i.e.

with  $\Delta t_i = 0$ . Then  $\varphi$  would be a harmonic mapping, yielding geodesic images, implying constant gradient length. Based on this, the requirements (62) and (63) should be straight forward.

To see why  $t_i$  can usually be considered a harmonic function, we think of  $\mathbf{g}_i$  as a Dirichlet problem under Von Neumann boundary conditions. If  $\mathbf{g}_i^{-1}(\min_i)$ ,  $\mathbf{g}_i^{-1}(\max_i)$  reside on the boundary – which is mostly the case –  $t_i$  is subject to a Dirichlet boundary condition in these areas. Otherwise, if one or several of these extrema are in the interior of  $\mathcal{V}$ , remove a surrounding  $\epsilon$  ball to form a boundary, yielding the potential as Dirichlet boundary conditions.  $t_i$  must still fulfill Von Neumann boundary conditions where level sets hit the boundary orthogonally. Thus, the slowest  $t_i$  can be obtained from solving a Dirichlet problem under mixed boundary conditions, also known as *Zaremba's problem*. In [Brown, 1994] solutions of such problems are studied on Lipschitz domains. They find that if a solution exists, it is a harmonic function. However, it is stated that a solution only exists if the different types of boundary conditions are separated by non-smooth points on the boundary such that they meet at an angle strictly smaller than  $\pi$ . This matches our experimental observations where  $\mathbf{g}_i^{-1}(\min_i)$ ,  $\mathbf{g}_i^{-1}(\max_i)$  always fill entire edges of the boundary in such a way. Alternatively we observe single-point extrema in some corners. Note that this observation may be biased as in an empirical exploration phase, the point in a corner has probability zero. Under analytic view, in such a case the area of Dirichlet boundary condition is a null set and thus not in scope of the setting in [Brown, 1994].

From theorem 2 we conjecture that some points  $\mathbf{a} \in \mathbf{g}_1^{-1}(\min_1)$ ,  $\mathbf{b} \in \mathbf{g}_1^{-1}(\max_1)$  realize the intrinsic geodesic diameter of  $\mathcal{V}$ . One might expect that in domains with boundary, this maximal intrinsic diameter is always realized by points on the boundary. There actually exist counter examples for multiply connected domains. In [Bae et al., 2013] such examples are given for polygonal domains in the plane. It is however stated that for simply connected polygons the diameter is always realized by some vertex points. This should be true for general simply connected domains with boundary, but a reference for this is hard to find. At least for convex domains it is somewhat obvious, because the diameter is always a straight line and there exists a cutting plane on which the problem of finding the diameter reduces to the two dimensional case. Since a smooth domain in the plane can be approximated by a polygon, the result for polygons transfers to this case.

Before we can start with the proof of theorem 2, we need the following lemma:

**Lemma 2**

For  $k > 0$ , on an  $n$ -dimensional surface  $\mathcal{S}$  the variational optimization problem

$$\underset{f: \mathcal{S} \rightarrow \mathbb{R}}{\text{minimize}} \quad \int_{\mathcal{S}} \frac{1}{f^k(\mathbf{x})} dV \tag{64}$$

$$\text{subject to} \quad \int_{\mathcal{S}} f(\mathbf{x}) dV = C \tag{65}$$

$$f(\mathbf{x}) > 0 \quad \forall \mathbf{x} \in \mathcal{S} \tag{66}$$

is solved by

$$f(x) \equiv \frac{C}{\text{vol}(\mathcal{S})} \tag{67}$$

Consequently we have  $\int_{\mathcal{S}} f^{-k}(\mathbf{x}) dV = \frac{\text{vol}(\mathcal{S})^{(k+1)}}{C^k}$

*Proof of Lemma 2.* We apply Euler-Lagrange equations with a Lagrange multiplier for the con-

straint (65):

$$\mathcal{L}(\mathbf{x}, \lambda, f, Df) = f^{-k}(x) + \lambda f(x) \quad (68)$$

$$\frac{\partial \mathcal{L}}{\partial f} = \sum_{j=1}^n \frac{\partial}{\partial \mathbf{x}_j} \frac{\partial \mathcal{L}}{\partial \left( \frac{\partial f}{\partial \mathbf{x}_j} \right)} = 0 \quad (69)$$

Since  $\mathcal{L}$  does not depend on derivatives of  $f$ , (69) is equal to zero. Inserting (68) into (69) yields

$$-\frac{k}{f^{k+1}}(\mathbf{x}) + \lambda = 0 \quad (70)$$

$$f(\mathbf{x}) = \left( \frac{k}{\lambda} \right)^{\frac{1}{k+1}} \quad (71)$$

This readily shows that  $f$  must be constant. (66) implies  $\lambda > 0$  in (70) and thus asserts that (71) yields a real number. We do not need to calculate  $\lambda$  explicitly, since the constant value of  $f$  is directly given by (65). Knowing  $f$  is constant, we have

$$(65) = \text{vol}(\mathcal{S})f(\mathbf{x}) = C \quad (72)$$

□

*Proof of Theorem 2.* We begin with the ansatz from (48):

$$\langle (\nabla \mathbf{g}_i(\mathbf{s}) \dot{\mathbf{s}})^2 \rangle_{\mathbf{s}, \dot{\mathbf{s}}} = \int_{\mathcal{V}} p_{\mathbf{s}}(\mathbf{s}) (D\mathbf{g}_i)(\mathbf{s}) \underbrace{\langle \dot{\mathbf{s}} \dot{\mathbf{s}}^T \rangle_{\dot{\mathbf{s}}|\mathbf{s}}}_{=: \mathbf{K}(\mathbf{s})} (D\mathbf{g}_i)^T(\mathbf{s}) dV \quad (73)$$

We consider the integral curves  $\varphi \in R_i$  of  $t_i$ , parameterized by arc length with the unit interval  $I$  as parameter space. Thus, the velocity  $|\nabla \varphi|_{\mathbf{G}}$  does not depend on  $\theta$ . By (62) we can assume that the gradients of  $t_i$  have the same property and considering the parameter spaces and images of  $\varphi$  and  $t_i$  we have

$$t(\mathbf{s}) = \varphi^{-1}(\mathbf{s}) \quad \forall \mathbf{s} \in \varphi(I) \quad (74)$$

This further yields  $|(\nabla t_i)(\varphi(\theta))|_{\mathbf{G}^{-1}} = \frac{1}{|\nabla \varphi(\theta)|_{\mathbf{G}}}$  and the calculus (73) continues as follows:

$$(73) = \int_{\mathcal{V}} p_{\mathbf{s}}(\mathbf{s}) (D\mathbf{g}_i)(\mathbf{s}) \mathbf{G}^{-1}(\mathbf{s}) (D\mathbf{g}_i)^T(\mathbf{s}) dV \quad (75)$$

$$= \int_{\mathbf{I}_{R_i}} \int_I p_{\mathbf{s}}(\varphi_{\mathbf{r}}(\theta)) \frac{(D\tilde{\mathbf{g}}_i)^2}{|\nabla \varphi_{\mathbf{r}}(\theta)|_{\mathbf{G}}^2} |\nabla \varphi_{\mathbf{r}}(\theta)|_{\mathbf{G}} g(\nabla^{\perp} \varphi_{\mathbf{r}}) d\theta d\mathbf{r} \quad (76)$$

$$= \int_{\mathbf{I}_{R_i}} \int_I \frac{1}{|\nabla \varphi_{\mathbf{r}}(\theta)|_{\mathbf{G}}} (D\tilde{\mathbf{g}}_i)^2 p_{\mathbf{s}}(\varphi_{\mathbf{r}}(\theta)) g(\nabla^{\perp} \varphi_{\mathbf{r}}) d\theta d\mathbf{r} \quad (77)$$

$$\stackrel{(62)}{=} \int_{\mathbf{I}_{R_i}} \frac{1}{|\nabla \varphi_{\mathbf{r}}(\theta)|_{\mathbf{G}}} d\mathbf{r} \int_I (D\tilde{\mathbf{g}}_i)^2 \int_{\mathbf{I}_{R_i}} p_{\mathbf{s}}(\varphi_{\mathbf{r}}(\theta)) g(\nabla^{\perp} \varphi_{\mathbf{r}}) d\mathbf{r} d\theta \quad (78)$$

$$\stackrel{(63)}{=} \int_{\mathbf{I}_{R_i}} \frac{1}{L_{\mathbf{G}}(\varphi_{\mathbf{r}})} d\mathbf{r} \int_I p_{\theta}(\theta) (D\tilde{\mathbf{g}}_i)^2 d\theta \quad (79)$$

We can transform the constraint in a similar manner, yielding

$$\langle \mathbf{g}_i^2(\mathbf{s}) \rangle_{\mathbf{s}} = \int_{\mathbf{I}_{R_i}} |\nabla \varphi_{\mathbf{r}}(\theta)|_{\mathbf{G}} d\mathbf{r} \int_I p_{\theta}(\theta) (\tilde{\mathbf{g}}_i)^2 d\theta \quad (80)$$

SFA requires the term (80) to be constantly one. Both integrals yield a certain constant value for the ideal solution  $\mathbf{g}_i$ . Let  $C_{ir}^* = \int_{\mathbf{I}_{R_i}} |\nabla \varphi_{\mathbf{r}}(\theta)|_{\mathbf{G}} d\mathbf{r}$  and  $C_{i\theta}^* = \int_I p_{\theta}(\theta) (\tilde{\mathbf{g}}_i)^2 d\theta$  denote these ideal constants. Surely, the ideal solution must satisfy  $C_{ir}^* C_{i\theta}^* = 1$ . We can now consider (79), (80) to yield two independently solvable optimization problems:

$$\begin{aligned} & \underset{\varphi}{\text{minimize}} && \int_{\mathbf{I}_{R_i}} \frac{1}{L_{\mathbf{G}}(\varphi_{\mathbf{r}})} d\mathbf{r} \\ & \text{subject to} && \int_{\mathbf{I}_{R_i}} L_{\mathbf{G}}(\varphi_{\mathbf{r}}) d\mathbf{r} = C_{ir}^* \end{aligned} \quad (81)$$

$$\begin{aligned} & \underset{\tilde{\mathbf{g}}_i \in \mathcal{F}}{\text{minimize}} && \int_I p_{\theta}(\theta) (D\tilde{\mathbf{g}}_i)^2 d\theta \\ & \text{subject to} && \int_I p_{\theta}(\theta) (\tilde{\mathbf{g}}_i)^2 d\theta = C_{i\theta}^* \end{aligned} \quad (82)$$

In (82),  $p_{\theta}(\theta)$  is the volume of the level set, weighted by  $p_{\mathbf{s}}(\varphi(\theta))$ :

$$p_{\theta}(\theta) = p_{\mathbf{s}}(\varphi(\theta)) \text{vol}(\{ \mathbf{s} \in \mathcal{V} : \exists \varphi \in R_i : \varphi(\theta) = \mathbf{s} \}) \quad (83)$$

Problem (82) is an ordinary SFA problem for a given  $t_i$ , while problem (81) minimizes the dominant cost factor w.r.t. the choice of  $t_i$ . Since  $\tilde{\mathbf{g}}_i$  is an arbitrary differentiable function, we can expect that it can be chosen to compensate the distribution of  $p_{\mathbf{s}}(\varphi(\theta))$  in (82). Equivalently to the technique in the proof of theorem 1, the decorrelation constraint on  $\tilde{\mathbf{g}}_i$  is already resolved on coordinate level, i.e. is only a constraint on  $t_i$ . The unit variance constraint is also resolved because we formulated this for the ideal partition of  $C_{ir}^* C_{i\theta}^* = 1$  assumed to be known. Indeed we observe in experiments that larger level sets yield a flatter  $\mathbf{g}_i$ . For problem (81) we apply lemma 2 with  $k = 1$ ,  $f(\mathbf{r}) = \frac{1}{|\nabla \varphi_{\mathbf{r}}|_{\mathbf{G}}}$ ,  $\mathcal{S} = \mathbf{I}_{R_i}$ . This shows that the ideal curves  $\varphi$  are such that  $|\nabla \varphi_{\mathbf{r}}|_{\mathbf{G}}$  is constant and as large as possible. This implies that the ideal  $t_i$  is the one that yields the longest integral curves w.r.t.  $\mathbf{G}$ . A well-known fact from differential geometry is that the integral curves of a gradient field with constant gradient length are geodesics. Consequently, a constant  $|\nabla \varphi_{\mathbf{r}}|_{\mathbf{G}}$  would yield geodesic curves  $\varphi$ . Note that this case cannot be fulfilled for every  $\mathcal{V}$ . It only characterizes an attractor for the best solution w.r.t. what  $\mathcal{V}$  permits.

If we assume a normalization  $\text{vol}(\mathbf{I}_{R_i}) = 1$  and further assume that the integral curves cover a fixed volume  $C$ , i.e.  $\int_{\mathbf{I}_{R_i}} L_{\mathbf{G}}(\varphi_{\mathbf{r}}) d\mathbf{r} = \int_{\mathbf{I}_{R_i}} |\nabla \varphi_{\mathbf{r}}|_{\mathbf{G}} d\mathbf{r} = C$ , we obtain the minimal value of (81) as  $\int_{\mathbf{I}_{R_i}} \frac{1}{|\nabla \varphi_{\mathbf{r}}|_{\mathbf{G}}} d\mathbf{r} = \frac{1}{C}$ . This shows that the covered volume  $C$  should be as large as possible in order to minimize (81).  $\square$

Intuitively, theorem 2 states that  $\mathbf{g}_i^{-1}(\min_i)$  and  $\mathbf{g}_i^{-1}(\max_i)$  must be as distant as possible within  $\mathcal{V}$ , w.r.t. intrinsic distance. In the fashion of xSFA, this yields a hierarchical covering of  $\mathcal{V}$

by the components  $\mathbf{g}_i$ . The fact that  $\mathbf{g}_i$  are orthogonal in the sense of decorrelation suggests a connection to principal curves [Hastie and Stuetzle, 1989] and manifold learning. More specifically the relation of  $\mathbf{g}_i$ 's streamlines to geodesics suggests a connection to principal geodesic analysis (PGA), [Fletcher et al., 2004]. The central difference to PGA is however, that PGA finds geodesics emanating from a central mean location in  $\mathcal{V}$ . Depending on the application, this can be a limitation if  $\mathcal{V}$  consists of multiple branches. There are, however, more recent approaches in manifold learning to overcome the limitation of a central mean, e.g. [Hauberg, 2016]. A more systematical comparison to these approaches would certainly be an interesting future study.

### 3.3 Global navigation algorithm

Our main idea is to decompose the sensor signal into monotonic flows using the first harmonics obtained by xSFA. We can then navigate along each component subsequently into a global optimum. Because of monotonicity this can be achieved by local optimization provided by the PFAx algorithm.

In consistence with notation from xSFA we refer to the components as *sources* in this section. Note that our procedure will not necessarily encounter physical sources. With *sources* we rather refer to whatever xSFA discovers. E.g. consider vision input, where the sensor is composed of visual features emitted from opposed walls, yet visible in a single field of view at the same time. Moving closer to one wall will increase vision of that wall's features and decrease vision of the opposing wall's features. In other words, the walls as sources of visual features are not statistically independent. The geometrical analysis in section 3.2 suggests that SFA will in such a case identify the agent's position along a coordinate axis between the walls as a virtual source. We focus on such virtual sources, because they are well suited for navigation, even though they might not correspond to actual physical features or entities. The slowest of such sources usually corresponds to the longest geodesic path that can be fitted into the environment, e.g. connecting the most distant pair of rooms. This is sometimes called the intrinsic geodesic diameter of the environment. The underlying heuristic of this principle is that a sensory perception of a consistent environment can always be decomposed into components that behave like monotonic flows.

It turns out that connectedness of the level sets of the extracted xSFA components is a crucial property. In mathematical topology, functions with this property are called *monotone*. Such topologically monotone functions are particularly valuable for the presented approach as they connect any pair of points in  $\mathcal{V}$  by a strictly monotonic path w.r.t. the component's value, as far as the points reside on distinct level sets. Theorem 1 asserts a weaker form of this property for xSFA components and indeed we mostly discover components that are topologically monotone. So far, we observed only two causes for eventually disconnected level sets:

- approximately equally slow sources are mixed due to superposition principle
- a multiply connected domain can yield one connection component of a level set per connectivity path

A special subroutine will be required to handle the case of disconnected level sets. Another issue can be caused by very flat regions in some xSFA components as no local gradient significantly points into a direction. While – in theory – still monotonic yet rather flat, in practice we can encounter regions with a representation close to constant or even with a moderate noise. This is caused by numerical approximation of the analytic solution. We will also present a subroutine to deal with



this effect. The following algorithm is the basic approach that works well for topologically monotone xSFA components. Consider step 6 as a slot where we can plug in the mentioned subroutines.

**Algorithm 1**

*Task: Navigate the agent into a goal state  $\mathbf{x}^*$ .*

1. Apply PFAX to extract  $r$  manipulatable features (pre feature space).
2. Apply xSFA to decompose these features into sources  $\mathbf{s}_{\alpha i}$  (feature space).
3. Use the obtained extraction rules on  $\mathbf{x}^*$  to compute the equivalent goal  $\mathbf{s}^*$  in feature space.
4. For  $\alpha = 1, \dots, S$ :  
 While  $\sum_{\beta=1}^{\alpha} (\mathbf{s}_{\beta 1} - \mathbf{s}_{\beta 1}^*)^2 > \theta$ : Choose  $\mathbf{u}(t)$  to minimize  $\sum_{\beta=1}^{\alpha} (\mathbf{s}_{\beta 1} - \mathbf{s}_{\beta 1}^*)^2$ .  
 If we cannot reduce  $\sum_{\beta=1}^{\alpha} (\mathbf{s}_{\beta 1} - \mathbf{s}_{\beta 1}^*)^2$  by more than  $\tilde{\theta}$ : Goto 6.
5. End.
6. Report failure.

Note that for statistically independent sources it would be sufficient to directly minimize the cost function  $\sum_{\beta=1}^S (\mathbf{s}_{\beta 1} - \mathbf{s}_{\beta 1}^*)^2$  of the final iteration. Extending the sum gradually during navigation is – however – more stable if the sources were not accurately separated by xSFA.

It can happen that PFAX has to minimize a source for which the current state resides in an almost flat area, c.f. section A.2. Then it might not be possible to find a proper direction for local optimization. We add a routine to deal with flat areas by using higher harmonics:

**Subroutine 1**

*Task: Deal with flat areas.*

6. If coming from 4: Set  $j = 2$ .  
 While  $\sum_{\beta=1}^{\alpha} (\mathbf{s}_{\beta 1} - \mathbf{s}_{\beta 1}^*)^2 + \sum_{i=1}^j (\mathbf{s}_{\alpha i} - \mathbf{s}_{\alpha i}^*)^2 > \theta$ :  
 Choose  $\mathbf{u}(t)$  to minimize  $\sum_{\beta=1}^{\alpha} (\mathbf{s}_{\beta 1} - \mathbf{s}_{\beta 1}^*)^2 + \sum_{i=1}^j (\mathbf{s}_{\alpha i} - \mathbf{s}_{\alpha i}^*)^2$   
 If we cannot reduce  $\sum_{\beta=1}^{\alpha} (\mathbf{s}_{\beta 1} - \mathbf{s}_{\beta 1}^*)^2 + \sum_{i=1}^j (\mathbf{s}_{\alpha i} - \mathbf{s}_{\alpha i}^*)^2$  by more than  $\tilde{\theta}$ :  
 Repeat 6 with  $j$  increased by 1.
7. Goto 4, i.e. perform another sweep.

We outlined the problem with disconnected level sets above. It can happen that the navigation reaches the right level set at the wrong connectivity component. This case can be detected by looking at other components. Then the heuristics is that, as xSFA fits as many orthogonal components into an environment as possible, every possible pair of points will be covered by some component such that the level sets run somewhat orthogonally to a path connecting the points.

Consider a multiply connected domain. We can split it into subdomains such that each subdomain is simply connected. Within a single subdomain, the level sets of an xSFA component are connected. If the issue was caused by superposition principle mixing two components, assume the

domain was split such that each section only contains connected level sets. We have no problem if the navigation task only concerns locations within one of these sections. However, note that each component would yield another kind of split. Thus, for tasks involving more than one section, we just have to find the right component, i.e. a component where our navigation task resides within the same section.

We formulate a subroutine based on this idea. First we detect that we are stuck by finding that the navigation is locally optimal, while the distance to the goal measured in feature space is still significantly high. We conclude that all components considered so far are not well suited for the current task in terms of level set connectivity. Starting at the current component, we search for a single component that yields significant improvement. After fully exploiting that component we must restart the algorithm at the first component, because this procedure has likely brought us to another connectivity component of the level sets considered so far. That means, all earlier components are now relevant again. We suppose that this procedure automatically avoids navigation cycles, because components are ordered by slowness.

### Subroutine 2

*Task: Deal with disconnected level sets.*

6. For  $\beta = \alpha, \dots, S$ :  
 While  $(\mathbf{s}_{\beta 1} - \mathbf{s}_{\beta 1}^*)^2 > \theta$ : Choose  $\mathbf{u}(t)$  to minimize  $(\mathbf{s}_{\beta 1} - \mathbf{s}_{\beta 1}^*)^2$ .  
 If this reduced  $(\mathbf{s}_{\beta 1} - \mathbf{s}_{\beta 1}^*)^2$  by more than  $\tilde{\theta}$ : Goto 4, i.e. perform another sweep.
7. Report failure.

To combine routines 1 and 2 we suggest to handle flat areas first. A new parameter  $j_{\max}$  is required as a termination condition of the first routine. This results in the combined routine

### Subroutine 3

*Task: Combined routine to deal with flat areas and disconnected level sets.*

6. If coming from 4: Set  $j = 2$ .  
 While  $\sum_{\beta=1}^{\alpha} (\mathbf{s}_{\beta 1} - \mathbf{s}_{\beta 1}^*)^2 + \sum_{i=1}^j (\mathbf{s}_{\alpha i} - \mathbf{s}_{\alpha i}^*)^2 > \theta$ :  
 Choose  $\mathbf{u}(t)$  to minimize  $\sum_{\beta=1}^{\alpha} (\mathbf{s}_{\beta 1} - \mathbf{s}_{\beta 1}^*)^2 + \sum_{i=1}^j (\mathbf{s}_{\alpha i} - \mathbf{s}_{\alpha i}^*)^2$   
 If we cannot reduce  $\sum_{\beta=1}^{\alpha} (\mathbf{s}_{\beta 1} - \mathbf{s}_{\beta 1}^*)^2 + \sum_{i=1}^j (\mathbf{s}_{\alpha i} - \mathbf{s}_{\alpha i}^*)^2$  by more than  $\tilde{\theta}$ :  
 If  $j < j_{\max}$ : Repeat 6 with  $j$  increased by 1, else goto 8.
7. Goto 4, i.e. perform another sweep.
8. For  $\beta = \alpha, \dots, S$ :  
 While  $(\mathbf{s}_{\beta 1} - \mathbf{s}_{\beta 1}^*)^2 > \theta$ : Choose  $\mathbf{u}(t)$  to minimize  $(\mathbf{s}_{\beta 1} - \mathbf{s}_{\beta 1}^*)^2$ .  
 If this reduced  $(\mathbf{s}_{\beta 1} - \mathbf{s}_{\beta 1}^*)^2$  by more than  $\tilde{\theta}$ : Goto 4, i.e. perform another sweep.
9. Report failure.

Finding  $S$  sources using xSFA involves  $S$  runs of ordinary SFA plus a significant amount of computation to generate and filter nonlinearities of already obtained sources. We propose a modified approach that requires only one single ordinary SFA run.

The central observation to achieve this is that once  $(\mathbf{s}_{\alpha 1} - \mathbf{s}_{\alpha 1}^*)^2$  is globally minimal, also  $(\mathbf{s}_{\alpha i} - \mathbf{s}_{\alpha i}^*)^2 \forall i > 1$  are globally minimal, at least if  $\mathbf{x}^*$  is a position that actually exists in the environment and not an artificial goal. Remember that each output component  $\mathbf{g}_i$  of plain SFA is composed of harmonics  $\mathbf{s}_{\alpha i}$  of earlier obtained sources. The first component found by SFA is however not a mixture, but the first harmonic of the slowest source, i.e.  $\mathbf{g}_1 = \mathbf{s}_{11}$ , assuming that  $\alpha = 1$  indicates the slowest source. Once we have globally minimized  $(\mathbf{g}_1 - \mathbf{s}_{11}^*)^2 = (\mathbf{s}_{11} - \mathbf{s}_{11}^*)^2$ , any further improvement potential in  $\mathbf{g}_j$  for  $j > 1$  must stem from a source with  $\alpha > 1$ . That means, we can alternatively optimize along  $\mathbf{g}_i$  subsequently instead of  $\mathbf{s}_{\alpha 1}$ :

### Algorithm 2

*Task: Navigate the agent into a goal state  $\mathbf{x}^*$ .*

1. Apply PFAx to extract  $r$  manipulatable features (pre feature space).
2. Apply SFA to decompose these features into  $R$  mixtures  $\mathbf{g}_i$  of sources (feature space).
3. Use the obtained extraction rules on  $\mathbf{x}^*$  to compute the equivalent goal  $\mathbf{g}^*$  in feature space.
4. For  $j = 1, \dots, R$ :  
 While  $\sum_{i=1}^j (\mathbf{g}_i - \mathbf{g}_i^*)^2 > \theta$ : Choose  $\mathbf{u}(t)$  to minimize  $\sum_{i=1}^j (\mathbf{g}_i - \mathbf{g}_i^*)^2$ .  
 If PFAx cannot reduce  $\sum_{i=1}^j (\mathbf{g}_i - \mathbf{g}_i^*)^2$  by more than  $\tilde{\theta}$ : Goto 6.
5. End.
6. Report failure.

We translate the routine for flat areas to this notion:

### Subroutine 4

*Task: Deal with flat areas.*

6. If coming from 4: Increase  $j$  by 1.  
 While  $\sum_{i=1}^j (\mathbf{g}_i - \mathbf{g}_i^*)^2 > \theta$ : Choose  $\mathbf{u}(t)$  to minimize  $\sum_{i=1}^j (\mathbf{g}_i - \mathbf{g}_i^*)^2$ .  
 If PFAx cannot reduce  $\sum_{i=1}^j (\mathbf{g}_i - \mathbf{g}_i^*)^2$  by more than  $\tilde{\theta}$ : Repeat 6 with  $j$  increased by 1.
7. Goto 4, i.e. perform another sweep.

The routine to handle disconnected level sets translates as follows:

### Subroutine 5

*Task: Deal with disconnected level sets.*

6. For  $i = j, \dots, R$ :  
 While  $(\mathbf{g}_i - \mathbf{g}_i^*)^2 > \theta$ : Choose  $\mathbf{u}(t)$  to minimize  $(\mathbf{g}_i - \mathbf{g}_i^*)^2$ .  
 If this reduced  $(\mathbf{g}_i - \mathbf{g}_i^*)^2$  by more than  $\tilde{\theta}$ : Goto 4, i.e. perform another sweep.
7. Report failure.

We conclude this section by providing the combined routine for algorithm 2. Here we do not need the parameter  $j_{\max}$ , because we can use  $R$  instead.

**Subroutine 6**

*Task: Combined routine to deal with flat areas and disconnected level sets.*

6. *If coming from 4: Set  $k = j + 1$ .  
While  $\sum_{i=1}^k (\mathbf{g}_i - \mathbf{g}_i^*)^2 > \theta$ : Choose  $\mathbf{u}(t)$  to minimize  $\sum_{i=1}^k (\mathbf{g}_i - \mathbf{g}_i^*)^2$ .  
If PFAx cannot reduce  $\sum_{i=1}^k (\mathbf{g}_i - \mathbf{g}_i^*)^2$  by more than  $\tilde{\theta}$ :  
If  $k < R$ : Repeat 6 with  $k$  increased by 1, else goto 8.*
7. *Goto 4, i.e. perform another sweep.*
8. *For  $i = j, \dots, R$ :  
While  $(\mathbf{g}_i - \mathbf{g}_i^*)^2 > \theta$ : Choose  $\mathbf{u}(t)$  to minimize  $(\mathbf{g}_i - \mathbf{g}_i^*)^2$ .  
If this reduced  $(\mathbf{g}_i - \mathbf{g}_i^*)^2$  by more than  $\tilde{\theta}$ : Goto 4, i.e. perform another sweep.*
9. *Report failure.*

## 4 Experiments and Applications

This section continues in a sense the experiments from [Richthofer and Wiskott, 2017], but using the global navigation technique developed in this paper. We solve the problematic obstacle scenario from there and also tackle even more complex multiroom scenarios. We start with a comprehension of the general navigation setting.

Inspired by reinforcement learning (RL) we have an agent in an environment – e.g. think of a virtual rat on a table. During a training phase it can explore the environment in order to solve navigation tasks. In contrast to RL we do not consider an arbitrary reward signal for now, but focus on navigating the agent into a desired goal state. In terms of RL this can be seen as using a distant function as reward signal, measuring the distance between the agent’s current state and the goal state. As distance measure we use least squares distance in feature space like it is denoted in the algorithms throughout section 3.3.

For exploration we assume a random walk with a fixed step size, choosing a new direction by a uniform random distribution after each step. A more sophisticated exploration routine could be applied in future work, e.g. curiosity-driven exploration by aiming for the largest change in the so far discovered slow feature space.

To model the sensory input signal we mostly focus on the wall sensor introduced in [Richthofer and Wiskott, 2017] – a virtual sensor that measures for a current location the visible fraction of each wall segment in an overall 360° field of view, see figure 7. E.g. for a plain square single room environment the sensor would emit four components, one for each wall. Note that because of the 360° field of view, the sensor is by construction invariant regarding head direction. This is a simplification, allowing us to focus on the navigation task itself. In [Franzius et al., 2007] it was shown that SFA is capable to find head direction invariant features, so this simplification is not a general restriction.

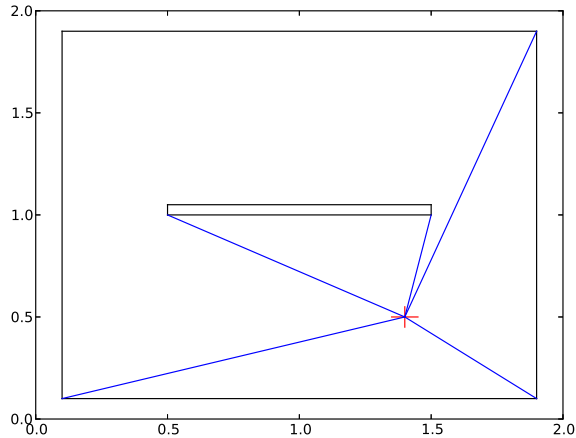


Figure 7: The full field of view is split up into sections occupied by each wall segment in a  $360^\circ$  field of view. The proposed wall sensor measures the fraction of each wall segment visible from the agent’s current location.

We apply a simplified version of PFAX in these experiments. If the relation between control signal and sensor signal is sufficiently simple, SFA can be used as a proxy for the extraction of predictable features. We applied (17) and (11) to obtain prediction matrices from an SFA extraction matrix. This is mainly done for technical simplicity as this simplification turned out to be sufficient for the experiments presented here. It was studied in [Weghenkel and Wiskott, 2018] that SFA often is a good proxy for extracting predictable features. Experiments concerning a complex control relationship that requires an actual dimensionality reduction in terms of PFAX may be part of future work.

For each environment studied in this section, we illustrate the features found by SFA, provide interpretations and discuss their suitability for navigation tasks. Then we illustrate how algorithm 2 would solve one or two exemplary navigation tasks by showing the paths that would arise during its first iterations. In these plots, the yellow crosshair always indicates the goal and the colormap displays Euclidean/least squares distance of each point to the goal in feature space. The navigation path is rendered in white on top of the colormap. Beyond that, we illustrate a vector field-like navigation flow for the whole environment in cyan. This is computed by performing a few navigation steps for each starting point on a uniform lattice across the whole environment. The environment’s bounding box is normalized to  $[0, 1]^2 \subset \mathbb{R}^2$  with preserved aspect ratio. Throughout this section we use an overly exhaustive training phase of 200000 steps. This shows that the algorithm cannot be over-trained and it yields very clean and interpretable results. We can sometimes even hypothesize that we gained results visually close to the unknown ideal SFA-solution for the respective environment. We start by examining the trivial case of a plain square single room.

## 4.1 SFA in two dimensions

For a better understanding of multi room experiments we first illustrate the features found by SFA in case of a single room environment. These are closely related to the harmonics shown in section 3.1.1. Especially the first two components in figure 8 are easily recognizable as the first harmonic along two distinct axes.

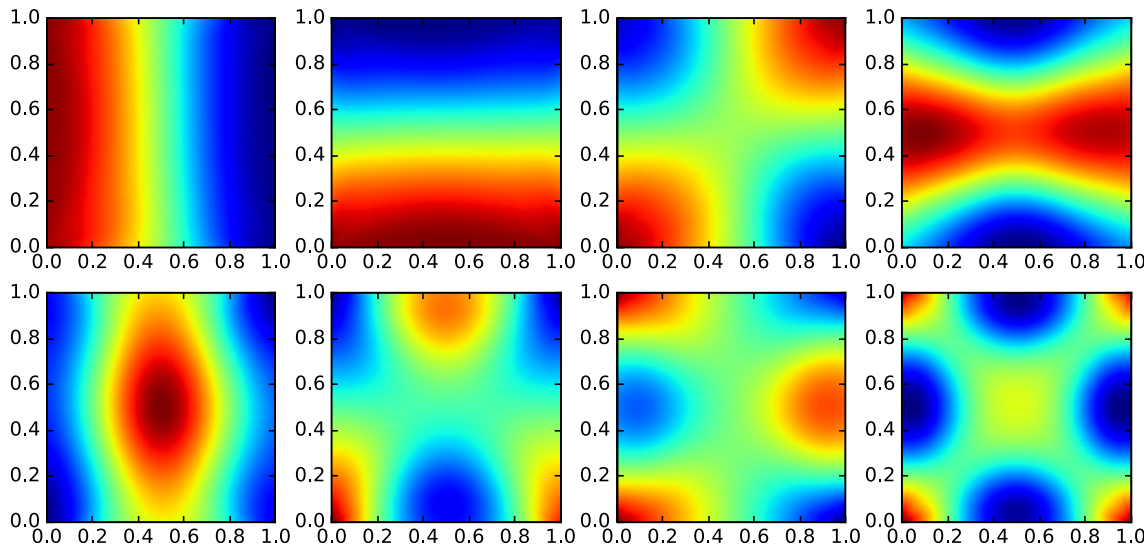


Figure 8: Illustration of SFA in two dimensions. The walk consists of 200k steps with random direction and fixed step size of 0.02. Nonlinear expansion was performed using monomials up to the fourth degree. The eight slowest components are shown.

We conclude that the algorithm recognizes the agent’s  $x$ -coordinate as the primary source because the slowest feature displays the first 1D harmonic laid out along the  $x$ -axis of the environment. The second feature displays the same harmonic along the  $y$ -axis, which is therefore the second source. Note that these features are almost equally slow and their order of appearance is arbitrary for a square environment. In a rectangular but non-square environment, the longest edge would yield the slowest source. Also their sign, i.e their direction of descent may be flipped. Subsequent components are mixtures of higher harmonics of these two sources and no third source can be discovered in this setting. We do not provide a navigation run for this setting, because it was already solved in [Richthofer and Wiskott, 2017].

In the following experiments this pattern will show up frequently in subregions, especially for each of the several rooms the complex environments are composed of. The pattern will however show some perturbation close to doors and other bottlenecks and will be augmented by more global features spanning several rooms.

## 4.2 Two rooms

We investigate the simplest case with multiple rooms. Figure 9 displays the eight slowest components for a symmetrical environment that is split into two rooms connected by a central pathway.

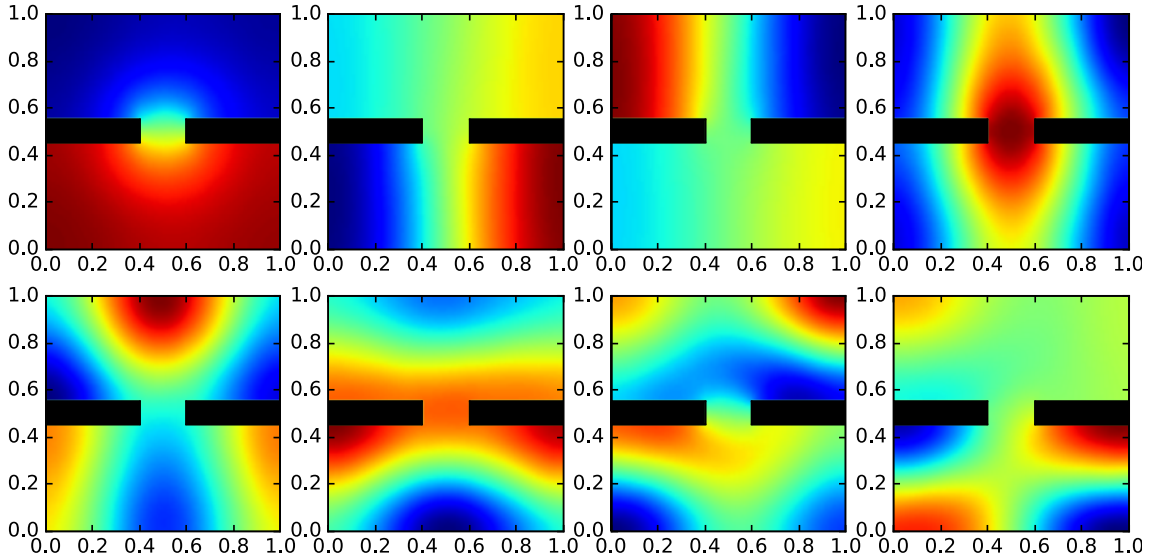


Figure 9: Illustration of SFA in two rooms. The walk consists of 200k steps with random direction and fixed step size of 0.02. Nonlinear expansion was performed using monomials up to the fifth degree. The eight slowest components are shown.

The first component is the slowest source and is the only source that spans both rooms. It is the crucial feature to navigate into the correct room and can even be seen as an indicator for room identity, linking this scenario to SFA based classification [Escalante-B. and Wiskott, 2013]. For our purpose, this component serves to guide the agent into the right room. Beneath its indicator characteristic the signal is still continuous and monotonically increasing/decreasing towards the pathway. Note the circular equipotential levels which serve to guide the agent to the door in case a room change is necessary.

The second and third components are equivalents of the first source we found in the previous section 4.1, but scoped on one room each. Indeed we would (more or less) find the whole decomposition from section 4.1 for each room over time. E.g. the eighth component corresponds to the third component from figure 8, scoped on the bottom room. The second component is an overlap of second harmonics of the sources. No further sources are discovered. All we find in subsequent components are mixtures of higher harmonics of the first three sources. The vertical component for each room is already provided by the first component as a side effect of its room-crossing nature. Compared to the pure vertical component in figure 8 it shows expectable perturbation at the pathway. Interestingly all three sources that exist in this environment are discovered almost cleanly unmixed, even though plain SFA was used and not xSFA. While we frequently observe rather unmixed initial occurrences of the first harmonics of the sources, this is not guaranteed. However, it is quite helpful for interpretation of the results.

The pathway itself is an attractor for steepness and we observe a similar perturbation of the harmonics as studied in section A.2. As concluded in that section this is not a big issue, but might require some special care if the signal should become too flat for proper navigation outside of the bottleneck. On the other hand there are use-cases for a detector of bottleneck states

([McGovern and Barto, 2001, Stolle and Precup, 2002]). A sudden increase of steepness in the first harmonic of each source can serve to detect such a bottleneck state, e.g. by applying a threshold on it's squared derivative. This principle can further be seen as a model for surprise, which is e.g. a central notion in [Schapiro et al., 2013].

The repeated occurrence of source characteristics and higher harmonics for each room is expectable as the rooms divide the environment into regions of low sensor correspondence. This observation supports the notion of a hierarchical decomposition of the environment into easier subtasks corresponding to independent sources.

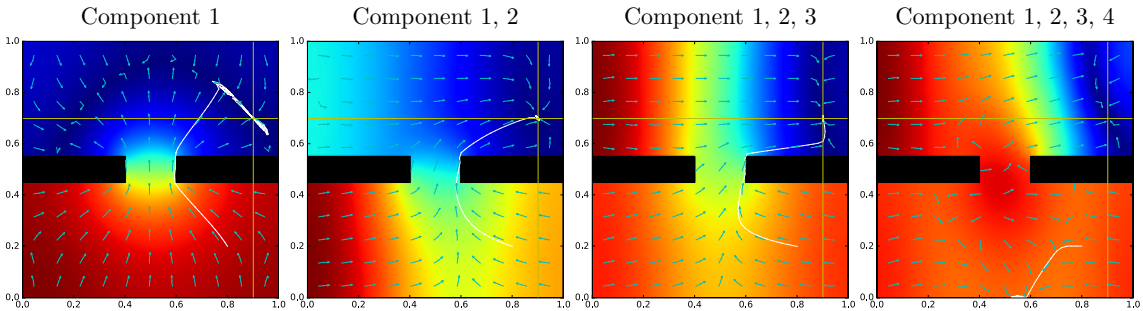


Figure 10: Illustration of SFA-based navigation using approximately independent sources. Combining the first three, i.e. the actual sources, yields successful navigation results. Adding a higher component right from the start would break navigation (right).

Figure 10 illustrates the combinations of sources the algorithm would use for navigation. Here we decompose the algorithm's iterations and navigate using only the sources from one iteration alone, thus illustrating its workability independently from  $\theta$ . Depending on  $\theta$  the navigation pathways would be merged. Note that when the algorithm would start to consider the fourth component, it would be already fairly close to the goal. The navigation failure of the fourth component in figure 10 only demonstrates that the component cannot be used right from the beginning.

#### 4.2.1 Using karthesian coordinates

As an alternative to the wall sensor we take a short look at learning the two-room-scenario based on plain karthesian  $(x, y)$ -coordinates as a sensor, e.g. like a GPS signal would provide. One might intuitively expect that navigation based on such coordinates is trivial. While this is the case for a single room, plain coordinates are particularly ill-suited for multiple rooms. Imagine two nearby spots, separated by a wall. Karthesian coordinates would poorly represent the fact that in terms of navigation these spots might be actually fairly distant.

An even more significant issue with this setting becomes clear once we remember that SFA obtained three sources describing this scenario. That means, with karthesian coordinates, our sensor would be lower dimensional than the number of sources forming our model, i.e.  $\dim(\mathbf{x}) < S$ . This is a rather strange relation: Instead of a manifold being embedded into a higher dimensional sensor space, it is now encoded into a lower dimensional space.

It turns out that SFA can still retrieve exactly the same sources that we previously found based on the wall sensor, but this requires an extremely high degree of nonlinear expansion. We start seeing the correct structures at expansion degrees between 30 and 40. Using monomials,



only expansion degrees  $< 20$  are numerically feasible with 64 bit floating point arithmetics. That means, this sensor representation requires a numerically more stable way of nonlinear expansion. Like in section A.2, we can leverage Legendre polynomials for this purpose.

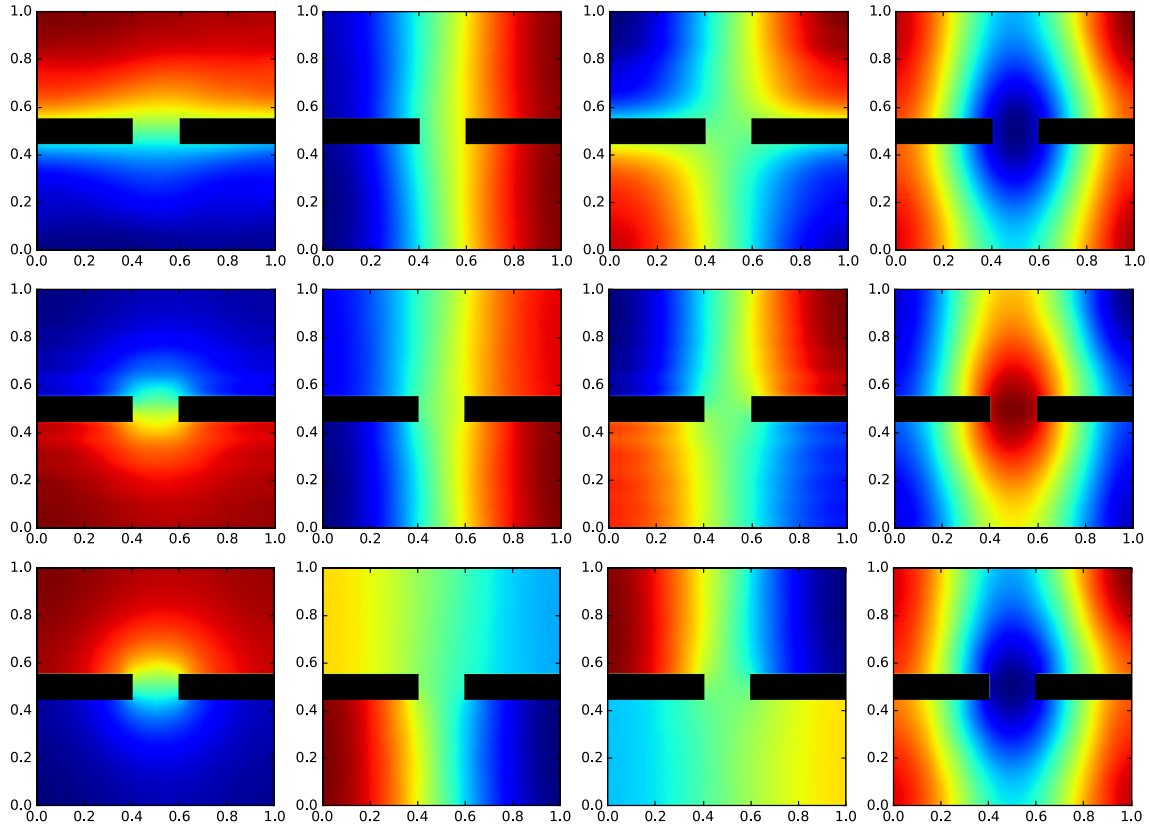


Figure 11: Illustration of SFA in two rooms based on karthesian coordinates as sensory input. The walk consists of 200k steps with random direction and fixed step size of 0.02. *Top*: Using monomials up to the 40th degree. *Center*: Using Legendre polynomials up to the 40th degree. *Bottom*: Using Legendre polynomials up to the 80th degree.

Figure 11 presents our results. Note that the top line, based on monomials up to the 40th degree, is visually approximately identical to monomials up to the 20th degree or Legendre polynomials up to the 20th degree. This illustrates the fact that monomials do not actually add new data representation from a certain degree onwards. Due to limited floating point precision they effectively compress all information to zero above that degree. As soon as we switch to Legendre polynomials, while keeping the same degree, we can clearly see how the features (center row) become closer to those based on the wall sensor in figure 9. Finally, using Legendre polynomials up to degree 80 or higher, we get approximately the same features as previously in figure 9. From this equivalence we conclude that the source-yielding components are visually close to the unknown ideal SFA-solutions of the two-room scenario. This hypothesis is supported by the high degree of

nonlinear expansion that was applied.

Besides demonstrating the advantage of Legendre polynomials for nonlinear expansion, figure 11 illustrates the transition from the single room case (Figure 8) to the two-room-case in figure 9. The lower the degree, the less perception for the wall is represented in the features.

### 4.3 Three rooms

In this section we study a more complex example. Our environment here consists of three rooms forking from a central corridor.

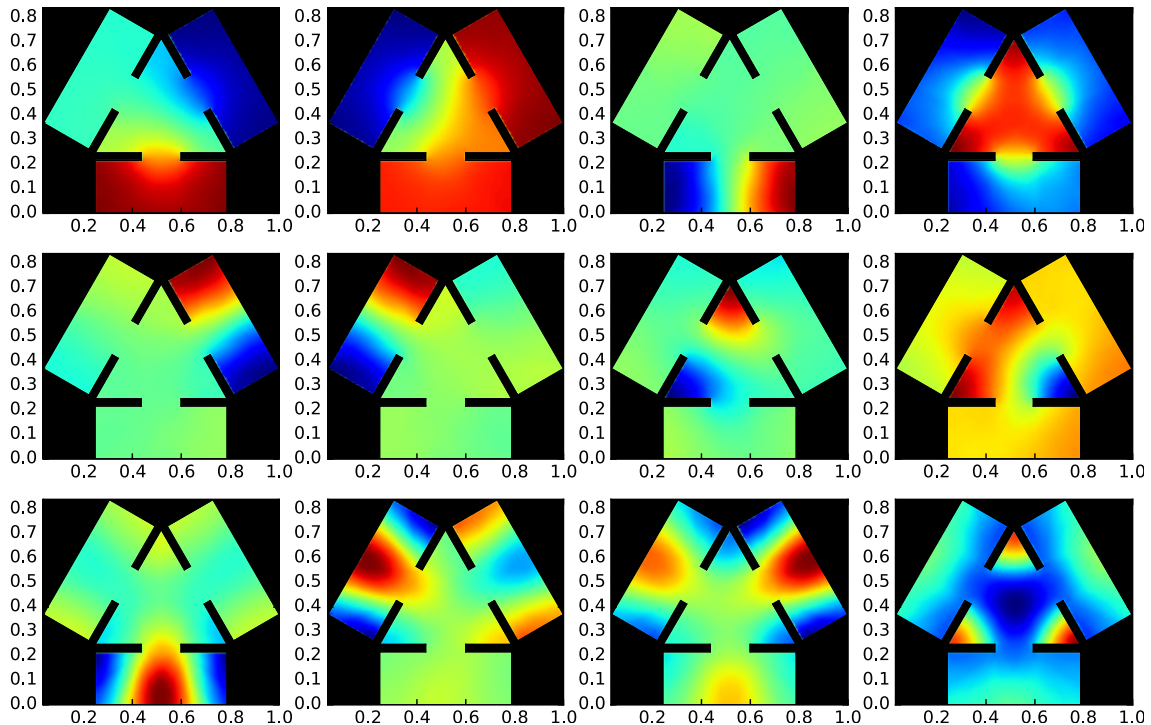


Figure 12: Illustration of SFA in three rooms with central corridor. The walk consists of 200k steps with random direction and fixed step size of 0.02. Nonlinear expansion was performed using monomials up to the second degree. The twelve slowest components are shown.

Figure 12 presents the features found by SFA. Like in the two-room example the first component is the slowest source and spans multiple rooms. It corresponds to the longest non-cyclic path that can be fitted into the environment. With non-cyclic we denote that the path must connect two points in environment space without detour. Note that the first component leaves one of the rooms plain. This is because each single source is a one-dimensional feature, embedded into a higher dimensional space. Thus it cannot span all three rooms in the given layout.

So, in contrast to the two room setting, we find the second component to span multiple rooms as well. It orthogonally connects the room that was previously plain with the path indicated by

the first component. However, the second source is not represented purely, but is intermixed with the second harmonic of the first source. Figure 13 demonstrates the logic behind algorithm 2 with subroutines, i.e. that navigation still succeeds in this case. The figure further asserts that the first two components are in combination sufficient to navigate into the right room from any starting point. The fourth component is an intermix of the second harmonics of the first two sources.

Components 3, 5 and 6 introduce the room-scoped sources we already found in earlier examples. We find the familiar pattern for each of the rooms, components 9, 10, 11 corresponding to the second harmonic of the room-internal sources.

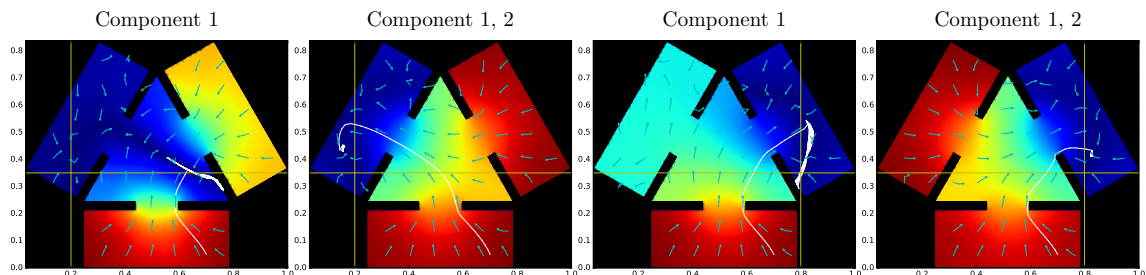


Figure 13: Illustration of SFA-based navigation using approximately independent sources. For two different tasks the navigation is displayed using only the first or the first two components.

To study the suitability of the obtained components for navigation, we present two tasks in figure 13: From bottom room to the left and from bottom room to the right. Given that the first source spans the bottom room and the right room, while leaving the left room flat, it can directly guide the agent from bottom to the right. To reach the left room, the second component is required, but the first one is still a useful prerequisite: It serves to guide the agent out of the starting room through the pathway into the corridor, settling it in front of the correct door. The second component is suitable to pull it into the room. Both navigation tasks would reach the goal position precisely if higher components were taken into account. In this demonstration we stopped after the second component, having the agent in the correct destination room, fairly close to the goal position.

#### 4.4 Four rooms

Extending the scenario by another room we can assert that the procedure scales well. The results here are friendlier for interpretation, because the number of rooms is a multiple of two. Since each source is one dimensional it can connect two rooms, allowing for an even split of the overall structure into sources. Figure 14 displays this effect in the sense that each source appears in a pair consisting of a horizontal and vertical counterpart. Note that SFA retrieves each source purely in this example. Due to the very clean and interpretable result, we hypothesize that the components shown in figure 14 are visually close to the unknown ideal SFA-solutions of this environment.

Like in the previous experiments we get some components that span multiple rooms (1, 2), later followed by room-internal sources (5, 6, 7, 8). Components 2 and 3 are mixtures of the second harmonics of the first two sources. The first two components correspond again to the longest non-cyclic paths that can be fitted into the environment.

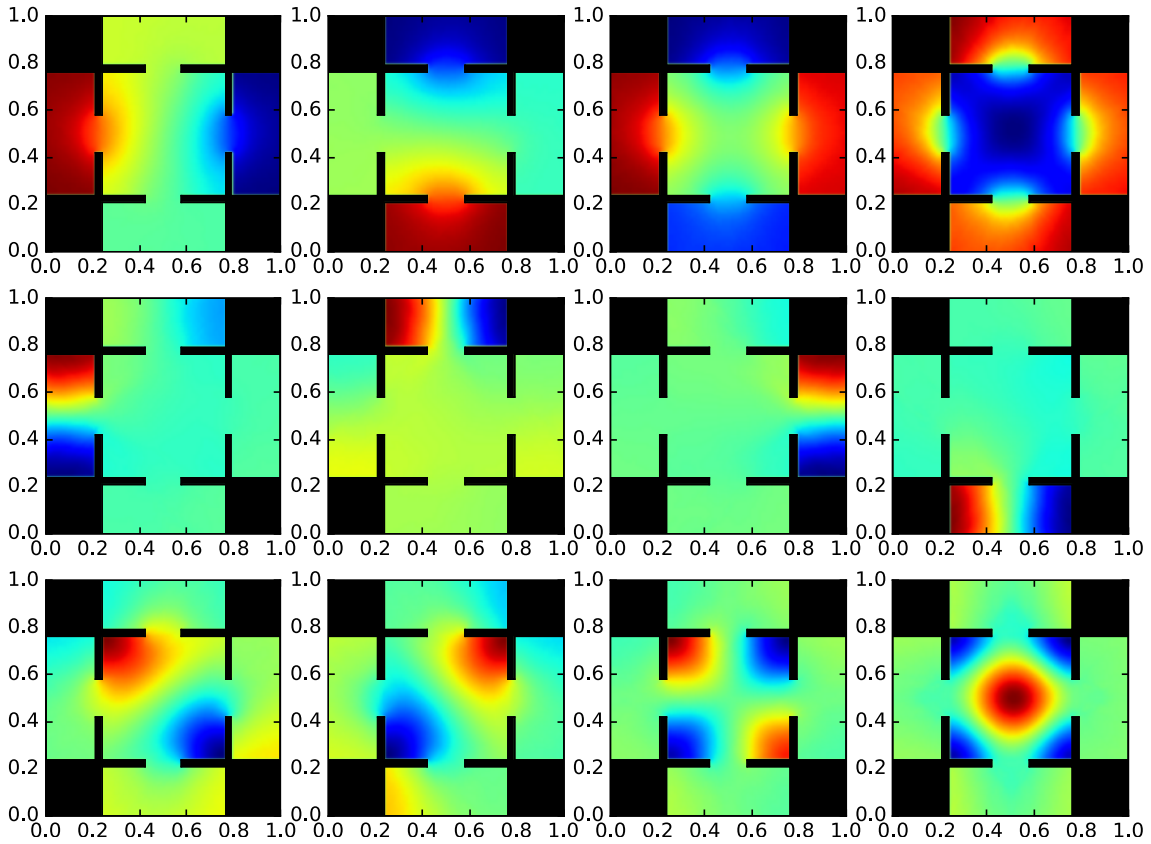


Figure 14: Illustration of SFA in four rooms with central corridor. The walk consists of 200k steps with random direction and fixed step size of 0.02. Nonlinear expansion was performed using monomials up to the second degree. The twelve slowest components are shown.

We illustrate two navigation tasks in figure 15, roughly equivalent to those from the three-room example. Navigation along one of the first sources guides the agent directly into the destination room, like the navigation from left to right shows. Navigating around the corner, e.g. from bottom to right is only feasible using two components.

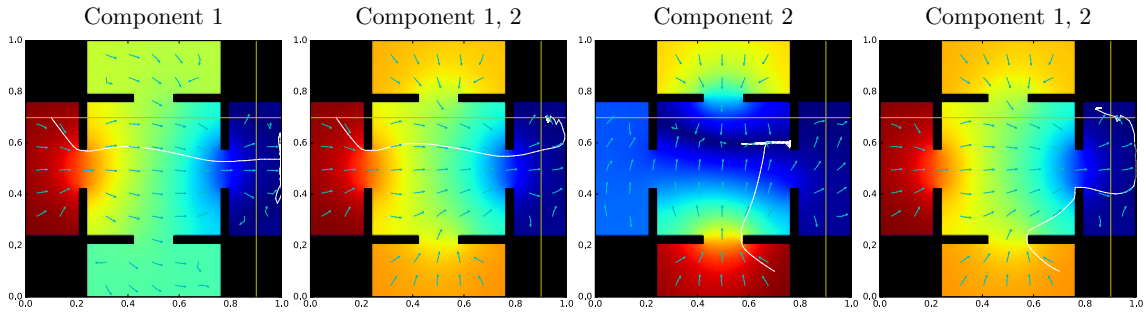


Figure 15: Illustration of SFA-based navigation using approximately independent sources. For two different tasks the navigation is displayed using only one or two components.

### 4.5 Three rooms, asymmetric

In this example we investigate a less symmetric arrangement of three rooms with a large rectangular corridor. Figure 17 illustrates clearly how the slowest source corresponds to the longest path that directly connects two points in the environment. It spans two rooms and the corridor, demonstrating that the rooms are not chosen arbitrarily but that it spans specifically the most distant rooms while leaving the central room plain.

The second source takes the formerly plain central room into account, yielding a mixture with the second harmonic of the first source across the rest of the environment. Yet again, the first two components are feasible to direct the agent into the destination room, which is illustrated by two navigation tasks in figure 16: Left to right and left to center. Like in the symmetric three-room example, the second component is required for entering the central room, which is flatly represented by the first component. Without the second component the agent is at least guided to the entrance of the destination room.

Due to the large corridor we must consider more components than in earlier examples, before we find the typical room-internal sources in components 12, 14 and 15 displayed in figure 17.

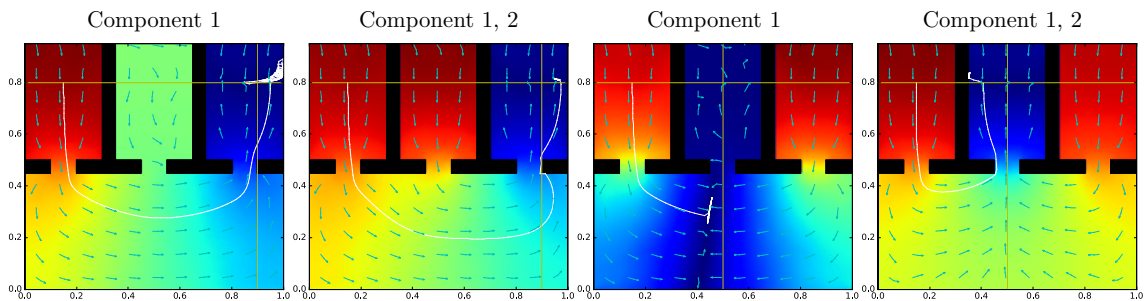


Figure 16: Illustration of SFA-based navigation using approximately independent sources. For two different tasks the navigation is displayed using only the first or the first two components.

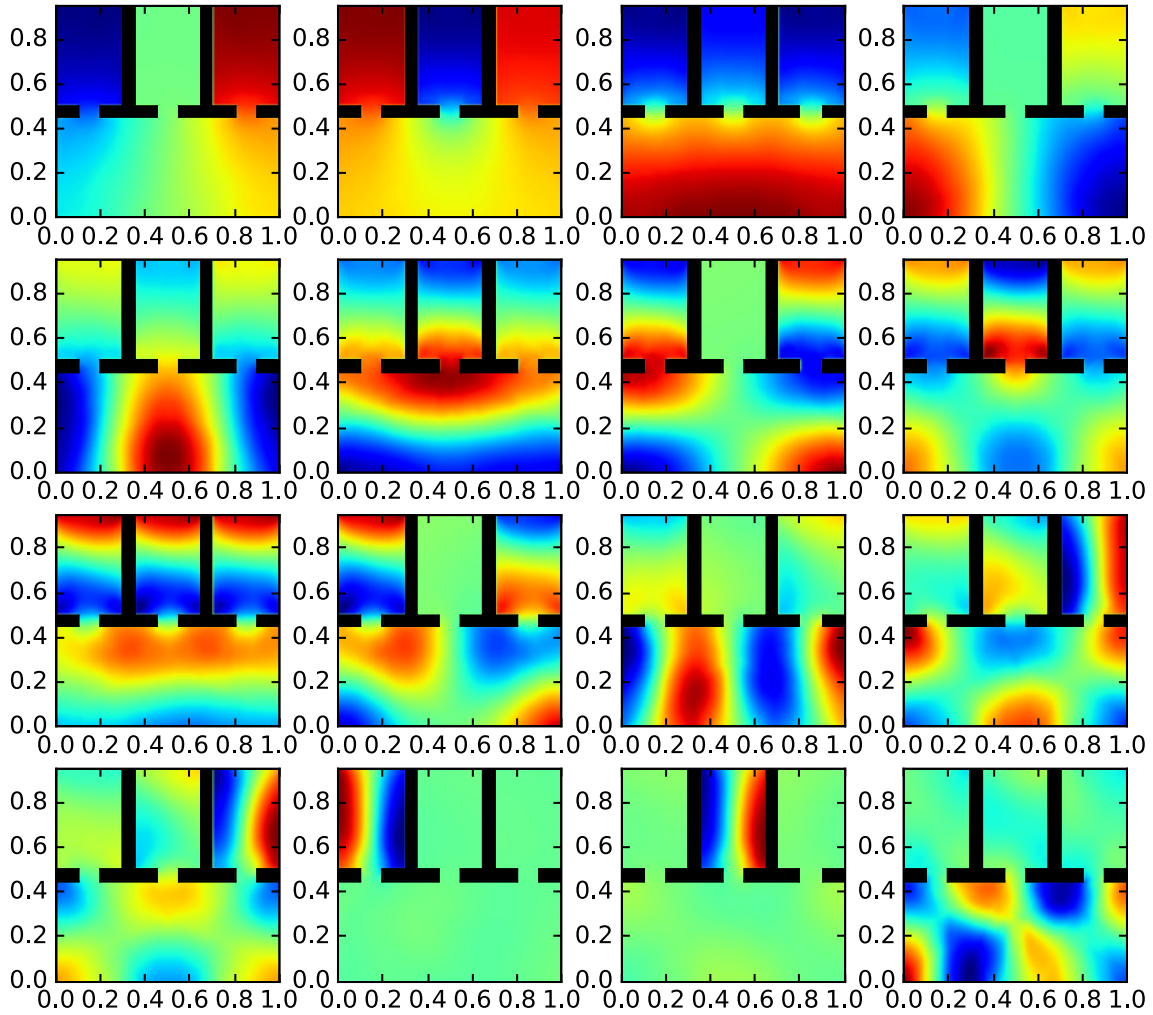


Figure 17: Illustration of SFA in three rooms with large corridor at the bottom. The walk consists of 200k steps with random direction and fixed step size of 0.02. Nonlinear expansion was performed using monomials up to the second degree. The sixteen slowest components are shown.

## 4.6 Navigation with obstacle

This example deals with the obstacle environment familiar from [Richthofer and Wiskott, 2017]. Figure 18 displays the first eight components. Indeed, the first component is suitable to guide an agent vertically around the obstacle if the navigation task requires it. In figure 19/left the navigation strives the obstacle because the obtained features were not sufficiently predictable. Note that the actual gradient would have avoided the obstacle. Predictability can be improved by using a higher expansion.

Surrounding the obstacle horizontally does not work based on the first component alone. A fundamental difference to the previous examples is that this environment yields no simply connected space. This issue manifests in the fact that the first source – while being monotonic – might still yield local optima for navigation. These can be circumvented by using higher components, but might in general require an additional routine for component selection.

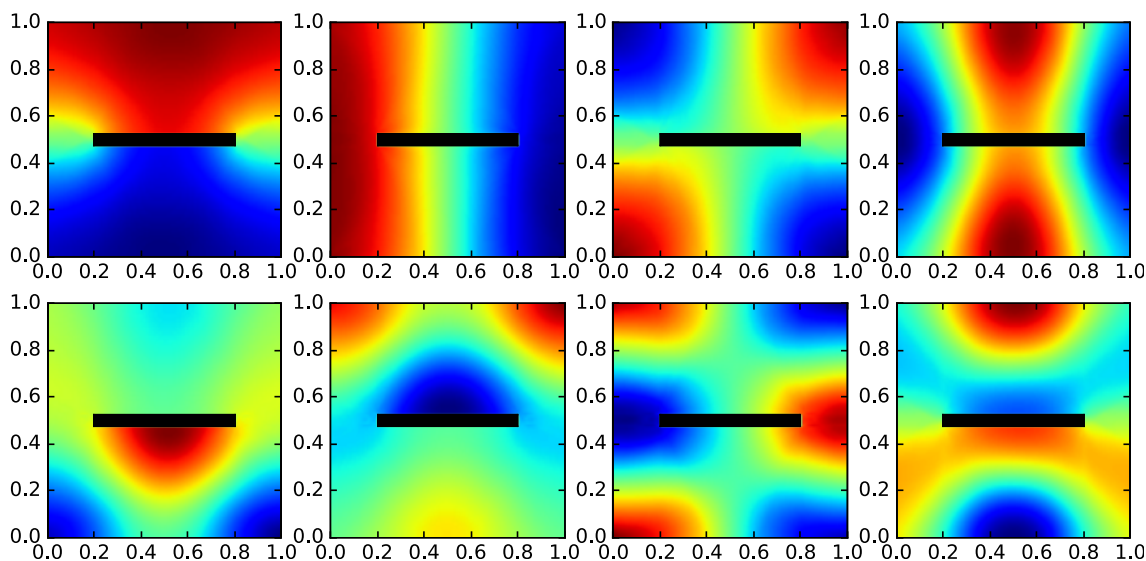


Figure 18: Illustration of SFA in an environment with obstacle. The walk consists of 200k steps with random direction and fixed step size of 0.02. Nonlinear expansion was performed using monomials up to the fourth degree. The eight slowest components are shown.

The effect is illustrated in figure 19/second, where we have an example where navigation along the first component ends up in the wrong state. Adding the second component solves the issue in this case (Figure 19/third), because it dominates and can guide the agent to the right destination.

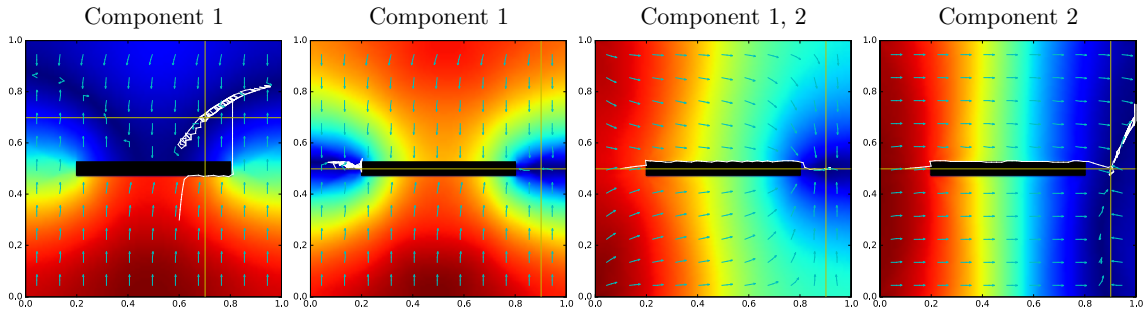


Figure 19: Illustration of SFA-based navigation around an obstacle for two navigation tasks. *Left*: Due to poor prediction the agent strikes the obstacle, but can still reach the goal. *Second*: The first component is not feasible to guide around the obstacle horizontally. *Third*: The second component dominates sufficiently to guide the agent around. *Right*: The second component alone would be sufficient in this case.

## 4.7 Pendulum swing-up with limited torque

We finally apply SFA to a dynamical system manipulation task. Pendulum swing-up with limited torque is a classical RL problem where the agent controls a harmonic pendulum by directly applying a torque to its fixpoint. The goal is to bring the pendulum into vertical stand-up position. The torque is limited such that the agent cannot simply turn up the pendulum, but has to swing it. With the goal being a specific destination state the reward function can be translated to our setting. We perceive the control task as a navigation task in the phase space of the pendulum. In this section we plot velocity on the  $x$  axis and angular amplitude on the  $y$  axis. The goal state is therefore at the center of the top boundary with maximum amplitude (pendulum pointing up) and zero velocity.

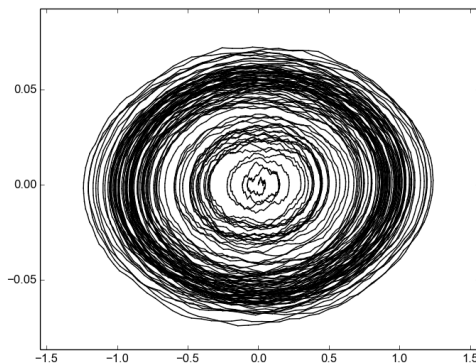


Figure 20: Phase space of a harmonic pendulum during training. The pendulum is controlled randomly over 10000 steps.



Data for the training phase is generated by controlling the pendulum randomly (Figure 20).

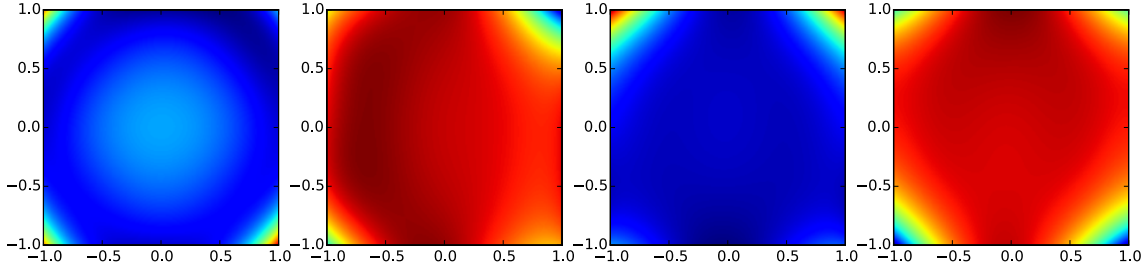


Figure 21: Illustration of SFA on the phase space of a harmonic pendulum. The four slowest components are shown.

The slowest component in figure 21 shows a clear representation of the circular nature of the training phase. Its gradient captures the rule that for reaching any position at the boundary it is crucial to walk away from the center into any direction. Navigating along the first component tells the agent to swing the pendulum, regardless of the precise goal location. Considering the higher components when a sufficient velocity is acquired, will settle in the specific goal state.

## 5 Discussion

### 5.1 Summary

We combined the unsupervised PFax and SFA algorithms to efficiently model a previously unknown environment in a way that is suitable for globally solving navigation and control tasks. PFax is used to utilize the command signal that controls the agent and to model a low dimensional space of well manipulatable features. SFA is applied on top of that to decompose the global structure of the environment into monotonic features that allow PFax-driven local navigation to find a global optimum.

To explain and support this decomposition, the monotonicity and geometrical properties of the obtained features, we extended mathematical theory of SFA and xSFA to manifolds. Former applications of SFA mainly exploited its ability to find invariances. In this work we explicitly utilize SFA-induced monotonicity as the link between local and global optimization.

In experiments of stepwise increased complexity we demonstrated how this principle scales to multiple rooms and leads to a hierarchical decomposition of the environment into components that yield globally solvable tasks. As soon as such a decomposition is achieved, it can be used to efficiently solve a whole range of tasks. The corresponding goal states do not need to be known during the training phase as the decomposition – if complete and sufficiently accurate – is suitable to solve for any possible goal state in the environment. Finally we demonstrated applicability to phase spaces of dynamical systems.

The whole procedure is engineered to fully consist of computationally efficient building blocks, most notably of eigenvalue decompositions. A remaining goal is to assemble a better scalable implementation, e.g. by applying PFax hierarchically or using incremental implementations of SFA and PFax. With this in line, the principle can be used on higher dimensional sensors and thus in more realistic and complex settings.

## 5.2 Conclusion and perspective

We conclude that SFA and PFAX can augment each other to form a framework for globally solving tasks that involve navigation and control. Especially SFA typically yields results that are well interpretable and can provide new insights into the structure of such a task. These insights are valuable beyond the computation of a solution. PFAX on the other hand provides insight into the relation between sensor and control signal.

Both building blocks – SFA and PFAX – are dimensionality reduction algorithms suitable to operate on approximately continuous signals. As such they form a promising approach to deal with the curse of dimensionality that traditionally affects the RL setting. Given that the described procedure is well scalable, e.g. by using a hierarchical or incremental setup, this framework can form the basis of an efficient and flexible engine for continuous reinforcement learning. Most notably, the method only needs to compute a single model – without having to know the actual goal state – and is finally capable to achieve any goal state based on this single model. This characteristic is especially valuable for use cases where the goal can suddenly change over time.

To cover the original RL setting, a better exploration method and incorporation of an arbitrary reward signal are still gaps to be closed.

- To improve exploration efficiency, the algorithm could operate in an online mode during exploration and choose exploration steps by curiosity, i.e. by aiming for the largest possible change of the agent’s current state in feature space.
- An arbitrary reward signal or its accumulation could be tracked as an additional sensor component during training phase. Later, the navigation goal could be formulated in terms of this sensor component.

In section 1 we mentioned some simplifying assumptions:

- The environment is fully observable, i.e. every position yields a unique representation in sensor space
- The environment is stationary, i.e. constant over time, contains no blinking lights, no flickering colors or moving objects

Fully observable does *not* mean that every pair of locations must be visible from each other. This was demonstrated in various scenarios involving multiple rooms, where the goal position is not visible from the starting position, see section 4.

The named limitations are not inherent and we can readily suggest extensions of the algorithm to overcome each of them:

- An environment with ambiguous sensor representations can be handled by time embedding or incorporating an episodic memory module into the sensor signal. Steepness in SFA components can be used – in sense of a model for surprise – to trigger memory write access.
- A time-dynamic environment can be handled by time embedding or by setting the time-order parameter of PFAX ( $p$ ) sufficiently high. To be feasible this would likely require a hierarchical PFAX implementation (c.f. hierarchical SFA, [Franzius et al., 2007, Schönfeld and Wiskott, 2015]).

Each of the proposals in this section would yield a significant extension to the algorithm and could fill a future publication on its own.

## **Acknowledgments**

This work is funded by a grant from the German Research Foundation (Deutsche Forschungsgemeinschaft, DFG) to L. Wiskott (SFB 874, TP B3) and supported by the German Federal Ministry of Education and Research within the National Network Computational Neuroscience - Bernstein Fokus: “Learning behavioral models: From human experiment to technical assistance”, grant FKZ 01GQ0951.

## References

- [Bae et al., 2013] Bae, S. W., Korman, M., and Okamoto, Y. (2013). The geodesic diameter of polygonal domains. *Discrete & Computational Geometry*, 50(2):306–329.
- [Berkes and Wiskott, 2002] Berkes, P. and Wiskott, L. (2002). Applying slow feature analysis to image sequences yields a rich repertoire of complex cell properties. In Dorronsoro, J. R., editor, *Artificial Neural Networks — ICANN 2002*, pages 81–86, Berlin, Heidelberg. Springer Berlin Heidelberg.
- [Böhmer et al., 2013] Böhmer, W., Grünewälder, S., Shen, Y., Musial, M., and Obermayer, K. (2013). Construction of approximation spaces for reinforcement learning. *Journal of Machine Learning Research*, 14:2067–2118.
- [Böhmer et al., 2015] Böhmer, W., Springenberg, J. T., Boedecker, J., Riedmiller, M. A., and Obermayer, K. (2015). Autonomous learning of state representations for control: An emerging field aims to autonomously learn state representations for reinforcement learning agents from their real-world sensor observations. *KI*, 29(4):353–362.
- [Botvinick et al., 2009] Botvinick, M. M., Niv, Y., and Barto, A. C. (2009). Hierarchically organized behavior and its neural foundations: A reinforcement learning perspective. *Cognition*, 113(3):262 – 280. Reinforcement learning and higher cognition.
- [Box and Tiao, 1977] Box, G. E. P. and Tiao, G. C. (1977). A canonical analysis of multiple time series. *Biometrika*, 64(2):pp. 355–365.
- [Brown, 1994] Brown, R. (1994). The mixed problem for laplace’s equation in a class of lipschitz domains. *Comm. Partial Diff. Eqns*, 19.
- [Engedy and Horvath, 2009] Engedy, I. and Horvath, G. (2009). Artificial neural network based mobile robot navigation. In *2009 IEEE International Symposium on Intelligent Signal Processing*, pages 241–246.
- [Escalante-B. and Wiskott, 2013] Escalante-B., A. N. and Wiskott, L. (2013). How to solve classification and regression problems on high-dimensional data with a supervised extension of Slow Feature Analysis. *Journal of Machine Learning Research*, 14:3683–3719.
- [Fletcher et al., 2004] Fletcher, P. T., Lu, C., Pizer, S. M., and Joshi, S. (2004). Principal geodesic analysis for the study of nonlinear statistics of shape. *IEEE Transactions on Medical Imaging*, 23(8):995–1005.
- [Franzius et al., 2007] Franzius, M., Sprekeler, H., and Wiskott, L. (2007). Slowness and sparseness lead to place-, head direction-, and spatial-view cells. In *Proc. 3rd Annual Computational Cognitive Neuroscience Conference, Nov. 1–2, San Diego, USA*, pages III–8.
- [Franzius et al., 2008] Franzius, M., Wilbert, N., and Wiskott, L. (2008). Invariant object recognition with slow feature analysis. In Kůrková, V., Neruda, R., and Koutník, J., editors, *Artificial Neural Networks - ICANN 2008*, pages 961–970, Berlin, Heidelberg. Springer Berlin Heidelberg.
- [Franzius et al., 2011] Franzius, M., Wilbert, N., and Wiskott, L. (2011). Invariant object recognition and pose estimation with slow feature analysis. *Neural Computation*, 23(9):2289–2323.

- [Garrido et al., 2006] Garrido, S., Moreno, L., Abderrahim, M., and Martin, F. (2006). Path planning for mobile robot navigation using voronoi diagram and fast marching. In *2006 IEEE/RSJ International Conference on Intelligent Robots and Systems*, pages 2376–2381.
- [Goerg, 2013] Goerg, G. (2013). Forecastable component analysis. In Dasgupta, S. and Mcallester, D., editors, *Proceedings of the 30th International Conference on Machine Learning (ICML-13)*, volume 28, pages 64–72. JMLR Workshop and Conference Proceedings.
- [Goldberger et al., 2004] Goldberger, J., Roweis, S. T., Hinton, G. E., and Salakhutdinov, R. (2004). Neighbourhood components analysis. In *Advances in Neural Information Processing Systems 17 [Neural Information Processing Systems, NIPS 2004, December 13-18, 2004, Vancouver, British Columbia, Canada]*, pages 513–520.
- [Hastie and Stuetzle, 1989] Hastie, T. and Stuetzle, W. (1989). Principal curves. *Journal of the American Statistical Association*, 84(406):502–516.
- [Hauberg, 2016] Hauberg, S. (2016). Principal curves on riemannian manifolds. *IEEE Transactions on Pattern Analysis and Machine Intelligence*, 38(9):1915–1921.
- [Igarashi, 2002] Igarashi, H. (2002). Path planning of a mobile robot by optimization and reinforcement learning. *Artificial Life and Robotics*, 6(1):59–65.
- [Jonschkowski and Brock, 2013] Jonschkowski, R. and Brock, O. (2013). Learning task-specific state representations by maximizing slowness and predictability. In *Proceedings of the 6th International Workshop on Evolutionary and Reinforcement Learning for Autonomous Robot Systems (ERLARS)*.
- [Kollar and Roy, 2008] Kollar, T. and Roy, N. (2008). Trajectory optimization using reinforcement learning for map exploration. *The International Journal of Robotics Research*, 27(2):175–196.
- [Kun Su and Hu, 2015] Kun Su, Y. W. and Hu, X. (2015). Robot path planning based on random coding particle swarm optimization. *International Journal of Advanced Computer Science and Applications(IJACSA)*, 6(4).
- [Lagoudakis et al., 2002] Lagoudakis, M. G., Parr, R., and Littman, M. L. (2002). Least-squares methods in reinforcement learning for control. In *Proceedings of the Second Hellenic Conference on AI: Methods and Applications of Artificial Intelligence, SETN '02*, pages 249–260, London, UK, UK. Springer-Verlag.
- [Luciw and Schmidhuber, 2012] Luciw, M. D. and Schmidhuber, J. (2012). Low complexity proto-value function learning from sensory observations with incremental slow feature analysis. In *Artificial Neural Networks and Machine Learning - ICANN 2012 - 22nd International Conference on Artificial Neural Networks, Lausanne, Switzerland, September 11-14, 2012, Proceedings, Part II*, pages 279–287.
- [Mahadevan and Maggioni, 2007] Mahadevan, S. and Maggioni, M. (2007). Proto-value functions: A laplacian framework for learning representation and control in markov decision processes. *Journal of Machine Learning Research*, 8(2169-2231):16.

- [Mattheij and Söderlind, 1987] Mattheij, R. and Söderlind, G. (1987). On inhomogeneous eigenvalue problems. i. *Linear Algebra and its Applications*, 88-89(Supplement C):507 – 531.
- [McGovern and Barto, 2001] McGovern, A. and Barto, A. G. (2001). Automatic discovery of subgoals in reinforcement learning using diverse density. In *Proceedings of the Eighteenth International Conference on Machine Learning (ICML 2001)*, Williams College, Williamstown, MA, USA, June 28 - July 1, 2001, pages 361–368.
- [Metka et al., 2017] Metka, B., Franzius, M., and Bauer-Wersing, U. (2017). Efficient navigation using slow feature gradients. In *2017 IEEE/RSJ International Conference on Intelligent Robots and Systems (IROS)*, pages 1311–1316.
- [Richthofer and Wiskott, 2015] Richthofer, S. and Wiskott, L. (2015). Predictable feature analysis. In *14th IEEE International Conference on Machine Learning and Applications, ICMLA 2015, Miami, FL, USA, December 9-11, 2015*, pages 190–196.
- [Richthofer and Wiskott, 2017] Richthofer, S. and Wiskott, L. (2017). PFAx: Predictable Feature Analysis to Perform Control. *ArXiv e-prints*.
- [Romero-Martí et al., 2016] Romero-Martí, D. P., Núñez-Varela, J. I., Soubervielle-Montalvo, C., and de-la Paz, A. O. (2016). Navigation and path planning using reinforcement learning for a roomba robot. In *2016 XVIII Congreso Mexicano de Robotica*, pages 1–5.
- [Schapiro et al., 2013] Schapiro, A. C., Rogers, T. T., Cordova, N. I., Turk-Browne, N. B., and Botvinick, M. M. (2013). Neural representations of events arise from temporal community structure. 16:486 EP –. Article.
- [Schönfeld and Wiskott, 2015] Schönfeld, F. and Wiskott, L. (2015). Modeling place field activity with hierarchical slow feature analysis. *Front Comput Neurosci*, 9:51. 26052279[pmid].
- [Singh et al., 1994] Singh, S. P., Barto, A. G., Grupen, R., and Connolly, C. (1994). Robust reinforcement learning in motion planning. In Cowan, J. D., Tesauero, G., and Alspector, J., editors, *Advances in Neural Information Processing Systems 6*, pages 655–662. Morgan-Kaufmann.
- [Sprague, 2009] Sprague, N. (2009). Predictive projections. In *IJCAI 2009, Proceedings of the 21st International Joint Conference on Artificial Intelligence, Pasadena, California, USA, July 11-17, 2009*, pages 1223–1229.
- [Sprague, 2014] Sprague, N. (2014). Contingent features for reinforcement learning. In *Artificial Neural Networks and Machine Learning - ICANN 2014 - 24th International Conference on Artificial Neural Networks, Hamburg, Germany, September 15-19, 2014. Proceedings*, pages 347–354.
- [Sprekeler, 2011] Sprekeler, H. (2011). On the relation of slow feature analysis and laplacian eigenmaps. *Neural Computation*, 23(12):3287–3302. PMID: 21105830.
- [Sprekeler and Wiskott, 2008] Sprekeler, H. and Wiskott, L. (2008). Understanding Slow Feature Analysis: a mathematical framework. Cognitive Sciences EPrint Archive (CogPrints).

- [Sprekeler et al., 2014] Sprekeler, H., Zito, T., and Wiskott, L. (2014). An extension of Slow Feature Analysis for nonlinear blind source separation. *Journal of Machine Learning Research*, 15:921–947.
- [Stachenfeld et al., 2014] Stachenfeld, K. L., Botvinick, M., and Gershman, S. J. (2014). Design principles of the hippocampal cognitive map. In Ghahramani, Z., Welling, M., Cortes, C., Lawrence, N. D., and Weinberger, K. Q., editors, *Advances in Neural Information Processing Systems 27*, pages 2528–2536. Curran Associates, Inc.
- [Stolle and Precup, 2002] Stolle, M. and Precup, D. (2002). Learning options in reinforcement learning. In Koenig, S. and Holte, R. C., editors, *Abstraction, Reformulation, and Approximation*, pages 212–223, Berlin, Heidelberg. Springer Berlin Heidelberg.
- [TAN et al., 2007] TAN, G.-Z., HE, H., and SLOMAN, A. (2007). Ant colony system algorithm for real-time globally optimal path planning of mobile robots. *Acta Automatica Sinica*, 33(3):279 – 285.
- [Vadakkepat et al., 2000] Vadakkepat, P., Tan, K. C., and Ming-Liang, W. (2000). Evolutionary artificial potential fields and their application in real time robot path planning. In *Proceedings of the 2000 Congress on Evolutionary Computation. CEC00 (Cat. No.00TH8512)*, volume 1, pages 256–263 vol.1.
- [Warren, 1989] Warren, C. W. (1989). Global path planning using artificial potential fields. In *Proceedings, 1989 International Conference on Robotics and Automation*, pages 316–321 vol.1.
- [Weghenkel et al., 2017] Weghenkel, B., Fischer, A., and Wiskott, L. (2017). Graph-based predictable feature analysis. *Mach. Learn.*, 106(9-10):1359–1380.
- [Weghenkel and Wiskott, 2018] Weghenkel, B. and Wiskott, L. (2018). Slowness as a proxy for temporal predictability: An empirical comparison. *Neural Computation*, 30(5):1151–1179.
- [Wiskott and Sejnowski, 2002] Wiskott, L. and Sejnowski, T. (2002). Slow Feature Analysis: unsupervised learning of invariances. *Neural Computation*, 14(4):715–770.
- [Xu et al., 2017] Xu, Q. L., Cai, M. M., and Zhao, L. H. (2017). The robot path planning based on ant colony and particle swarm fusion algorithm. In *2017 Chinese Automation Congress (CAC)*, pages 411–415.
- [Zuo et al., 2014] Zuo, B., Chen, J., Wang, L., and Wang, Y. (2014). A reinforcement learning based robotic navigation system. In *2014 IEEE International Conference on Systems, Man, and Cybernetics (SMC)*, pages 3452–3457.

# A Appendix

## A.1 Notation overview

This section gives an overview of the notation used in this paper.

$\mathbf{x}(t)$	denotes the raw input signal.
$\mathbf{u}(t)$	denotes the external information signal.
$\Omega_t$	$:= \{t_0, \dots, t_k\}$ denotes a discrete time sequence (considered as equidistant with step size normalized to 1). We usually refer to $\Omega_t$ as the <i>training phase</i> .
$\langle \mathbf{s}(t) \rangle_{t \in S}$	$:= \frac{1}{ S } \sum_{t \in S} \mathbf{s}(t)$ denotes the average of some signal $\mathbf{s}$ over a finite set $S$ . For $S = \Omega_t$ we just write $\langle \mathbf{s}(t) \rangle_t$ or even $\langle \mathbf{s} \rangle$ , if it is obvious, what unbound variable is targeted.
$\mathbf{h}(\mathbf{x})$	denotes the expansion function and usually consists of a set of monomials of low degree.
$\mathbf{z}(t)$	denotes $\mathbf{h}(\mathbf{x}(t))$ after sphering.
$\mathbf{m}(t)$	denotes the optimized output signal ( $\mathbf{m}$ for <i>model</i> ).
$n$	$:= \dim(\mathbf{h}(\mathbf{x}))$ denotes the number of components to be analyzed (after expansion).
$n_{\mathbf{u}}$	$:= \dim(\mathbf{u})$ denotes the number of components in $\mathbf{u}$
$r$	denotes the number of extracted components (“features”).
$\mathbf{A}, \mathbf{a}$	denotes the matrix (or vector if $r = 1$ ) holding the linear composition of the output-signal. We set $\mathbf{m}(t) = \mathbf{A}^T \mathbf{z}(t)$ .
$\mathbf{a}_i$	denotes the $i$ 'th column of $\mathbf{A}$ , so we can write $m_i(t) = \mathbf{a}_i^T \mathbf{z}(t)$ .
$O(n)$	$\subset \mathbb{R}^{n \times n}$ denotes the orthogonal group of dimension $n$ , i.e. $\forall \mathbf{A} \in O(n): \mathbf{A} \mathbf{A}^T = \mathbf{A}^T \mathbf{A} = \mathbf{I}$
$p$	denotes the number of recent signal-values involved in the prediction. We also call it the <i>prediction-order</i> .
$\mathbf{I}_{s,r}$	denotes the $s \times r$ identity matrix ( $s$ counting rows, $r$ counting columns). For $s = r$ this is a usual square identity, while in the non-square case it consists of a square identity block in the top or left area, filled up with zeros to fit the given shape.
$\mathbf{I}_r$	$:= \mathbf{I}_{n,r}$
$\mathbf{A}_r$	$:= \mathbf{A} \mathbf{I}_r$

Further more we sometimes use the Kronecker product  $\otimes$  and the vec-operator defined as follows:

For matrices  $\mathbf{A} \in \mathbb{R}^{m \times n}$  and  $\mathbf{B} \in \mathbb{R}^{k \times l}$  and with  $a_{ij}$  denoting the entries,  $\mathbf{a}_i$  the columns of  $\mathbf{A}$ :

$$\mathbf{A} \otimes \mathbf{B} := \begin{pmatrix} a_{11} \mathbf{B} & \cdots & a_{1n} \mathbf{B} \\ \vdots & \ddots & \vdots \\ a_{m1} \mathbf{B} & \cdots & a_{mn} \mathbf{B} \end{pmatrix} \in \mathbb{R}^{mk \times nl} \quad (84)$$

$$\text{vec}(\mathbf{A}) := \begin{pmatrix} \mathbf{a}_1 \\ \vdots \\ \mathbf{a}_n \end{pmatrix} \in \mathbb{R}^{mn} \quad (85)$$



Additionally, we sometimes make use of the following shortcut:

$$\underline{\mathbf{A}} := \mathbf{I}_{p,p} \otimes \mathbf{A} = \begin{pmatrix} \mathbf{A} & & \mathbf{0} \\ & \ddots & \\ \mathbf{0} & & \mathbf{A} \end{pmatrix} \quad (86)$$

$\underbrace{\hspace{10em}}_{p \text{ times } \mathbf{A}}$

## A.2 SFA harmonics concerning a bottleneck

When dealing with multiple rooms, we encounter the transition between rooms as bottlenecks in the environment, i.e. areas of low probability during a random exploration of the environment. In this section we study the results of SFA for the case that a source is not uniformly distributed, but concerns a bottleneck in the probability distribution. Using a normally-distributed repeller  $\eta(x)$ , we model a bottleneck situation on a one dimensional interval  $[a, b]$ , i.e. concerning only a single source  $\mathbf{s}_\alpha = x$ ,  $n = 1$ . Throughout this section we use the shortcut  $\mu_{ab} := \frac{a+b}{2}$ . We define

$$\eta_{\tau,\sigma}(x) := \text{sign}(x - \mu_{ab}) \frac{\tau}{\sqrt{2\pi\sigma^2}} e^{-\frac{(x-\mu_{ab})^2}{2\sigma^2}} \quad (87)$$

$$p_{\dot{x}|x}(\dot{x}|x) := \frac{1}{2\delta} \mathbf{1}_{[-\delta+\eta_{\tau,\sigma}(x), \delta+\eta_{\tau,\sigma}(x)]}(\dot{x}) \quad (88)$$

with  $\delta$  denoting the strength of the random walk and  $\tau$  denoting the strength of the repeller. Empirically we find that if  $\delta$  is sufficiently large,  $p(x)$  can be modeled as an accordingly scaled difference between a uniform and a normal distribution:

$$p_x(x) \approx \mathbf{1}_{[a,b]}(x) \left( \frac{1 + \tilde{\tau}(\text{erf}_{\mu_{ab},\tilde{\sigma}}(b) - \text{erf}_{\mu_{ab},\tilde{\sigma}}(a))}{b-a} - \frac{\tilde{\tau}}{\sqrt{2\pi\tilde{\sigma}^2}} e^{-\frac{(x-\mu_{ab})^2}{2\tilde{\sigma}^2}} \right) \quad (89)$$

with  $\text{erf}_{\mu_{ab},\sigma} = \int \frac{1}{\sqrt{2\pi\sigma^2}} \exp(-\frac{(x-\mu_{ab})^2}{2\sigma^2})$  denoting the cumulative density function of a normal distribution. Of course,  $\tilde{\tau}$  and  $\tilde{\sigma}$  depend on  $\tau$  and  $\sigma$ , but formulating the specific relationship would require a deeper study of the heterogeneous random walk induced by (88). Further, we find that  $\langle \dot{x}^2 \rangle_{\dot{x}|x} = \frac{\eta_{\tau,\sigma}(x)^3}{3\delta} + \delta\eta_{\tau,\sigma}(x)$  is not constant, which results in a difficult differential equation for the analytic SFA solutions. These aspects are out of scope of this paper, so we focus on empirical results.

To simulate an unrestricted function space we use Legendre polynomials rather than monomials for nonlinear expansion. Monomials lead to invalid solutions or failures already at expansion degrees around 15 due to their poor numerical properties concerning floating point arithmetics (dirty zero effect). Using Legendre polynomials we are able to retrieve valid solutions for degrees  $> 100$ . Depending on the data we were able to apply expansions up to degree 140.

From the results in figure 22 we conclude that a bottleneck in the probability distribution acts like an attractor for steepness on the SFA solutions. The original harmonics are perturbed by a sudden concentration of steepness at the bottleneck. This is exactly expected behavior, because the bottleneck is a low-weight region and steepness is a high-cost factor for SFA. So the algorithm uses the bottleneck to store as much of the overall cost as possible. As a consequence, regions outside the bottleneck become flatter. Especially the first harmonic can gain – while still being monotonic

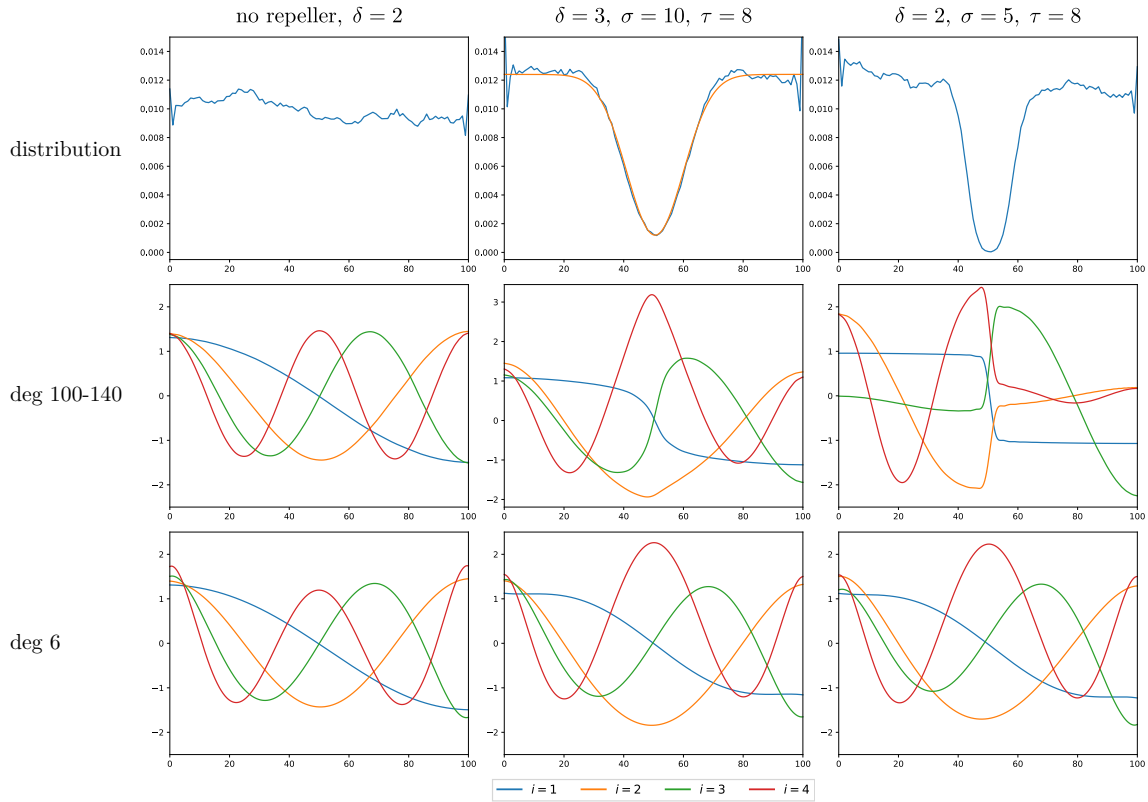


Figure 22: Illustration of SFA concerning a bottleneck. Each walk consists of  $10^6$  steps. For nonlinear expansion, Legendre polynomials up to the denoted degree were used: 100 in the center, 140 left and right. The second line displays approximately ideal solutions with a high nonlinear expansion simulating an unrestricted function space. The third line shows how solutions are smoothed due to a more restricted function space, i.e. Legendre polynomials up to the sixth degree.

– very flat regions, even close to constant. Thus, the first harmonic turns into an approximate indicator function distinguishing the two regions separated by the bottleneck. Also note that the sudden concentration of steepness can be used to detect the bottleneck state, which is a relevant notion in [McGovern and Barto, 2001, Stolle and Precup, 2002]. It can also model communities and surprise, which are relevant e.g. in [Schapiro et al., 2013].

For our navigation approach, flat regions can yield issues and we will propose a method to handle them. Note that – as illustrated in figure 22/bottom row – a more restricted function space has a smoothing effect on the solutions. This already compensates issues with flat regions to some extent.